

1 **A bidirectional network for appetite control in zebrafish**

2 ***Caroline Lei Wee**^{1,2,5}, ***Erin Yue Song**¹, Robert Evan Johnson^{1,2}, Deepak Ailani³, Owen
3 Randlett¹, Jiyeon Kim¹, Maxim Nikitchenko¹, Armin Bahl¹, Misha Ahrens⁴, Koichi Kawakami³,
4 Florian Engert¹ and **Samuel Kunes**¹

5 ***Equal contribution first authors**

6 ¹Department of Molecular and Cell Biology, Harvard University, Cambridge, MA, USA

7 ²Program in Neuroscience, Harvard University, Boston, MA, USA

8 ³Division of Molecular and Developmental Biology, National Institute of Genetics, Department of
9 Genetics, SOKENDAI (The Graduate University for Advanced Studies), Mishima, Shizuoka,
10 Japan

11 ⁴Howard Hughes Medical Institute, Janelia Farm Research Campus, Ashburn, Virginia, USA.

12 ⁵Institute of Molecular and Cell Biology, A*STAR, Singapore

13

14 **ABSTRACT**

15 Medial and lateral hypothalamic loci are known to suppress and enhance appetite, respectively,
16 but their interactions and dynamics have not yet been explored. Here we report that, in
17 zebrafish, serotonergic neurons of the ventromedial caudal hypothalamus (cH) becomes
18 increasingly active during food deprivation, whereas activity in the lateral hypothalamus (LH) is
19 reduced. Exposure to food sensory and consummatory cues reverses the activity states of
20 these two nuclei, reflecting an opposing internal hunger state induced by food. An intermediate
21 activity state is restored as satiety approaches. The overall antagonistic relationship of cH and
22 LH was confirmed by simultaneous calcium imaging, and a causal relationship was established
23 by targeted stimulation and ablation of the cH. The collective data allows us to propose a model
24 in which activities in anti-correlated hypothalamic nuclei direct distinct phases of hunger, and
25 thus coordinate energy balance via mutually antagonistic control of distinct behavioral outputs.

26

27 INTRODUCTION

28 The regulated intake of food based on caloric needs is a fundamental homeostatically controlled
29 process that is essential for health and survival. The hypothalamus is a highly conserved central
30 convergence point for the regulation of the neural and biochemical pathways underlying these
31 basic mechanisms. Early studies demonstrated by way of electrical stimulation or lesions that
32 specific hypothalamic regions play important roles in the regulation of appetite. For example,
33 while stimulation of ventromedial hypothalamic loci in rodents and cats reduced feeding,
34 activation of more lateral hypothalamic loci increased both hunting behavior and food intake
35 (ANAND and BROBECK, 1951; BROBECK et al., 1956; DELGADO and ANAND, 1953; Krasne,
36 1962). Conversely, lateral hypothalamic lesions were found to reduce feeding to the point of
37 starvation, whereas medial hypothalamic lesions resulted in overeating (ANAND and BROBECK,
38 1951; Hoebel, 1965; TEITELBAUM and EPSTEIN, 1962). Thus, the lateral and medial
39 hypothalamic regions came to be regarded as “hunger” and “satiety” centers, respectively.

40 Recent experiments employing optical and electrophysiological methods have lent
41 support to expectations based on these early studies. For example, GABAergic neurons in the
42 lateral hypothalamus were observed to be activated during feeding and essential for enhanced
43 food intake during hunger (Jennings et al., 2015; Stuber and Wise, 2016). However, these
44 experiments have examined only subsets of hypothalamic neurons; their activity patterns in the
45 context of the entire network remain unknown. This limited view hampers our understanding of
46 the dynamical interactions between the ensemble of brain circuits thought to be important for
47 the initiation, maintenance and termination of food consumption (Sternson and Eiselt, 2017).

48 Here, we leverage the small and optically accessible larval zebrafish to identify
49 modulatory regions central to the control of appetite and to shed light on their specific roles and
50 dynamical activity patterns in relation to the whole brain and behavior. Using pERK-based brain-
51 wide activity mapping we first identified neuronal populations that display differential neural
52 activity under conditions of hunger and satiety. We show that lateral and medial hypothalamic

53 regions have anti-correlated activity patterns during hunger, voracious feeding and satiety. Next,
54 through a combination of calcium imaging, optogenetics and ablation analysis, we show that
55 serotonergic neurons in the caudal periventricular zone of the medial hypothalamus (cH) are
56 state-dependent regulators of feeding behavior, likely via their modulation of the lateral
57 hypothalamus. This allows us to propose a model where mutually antagonistic brain states
58 regulate energy balance by encoding distinct signals in different facets of appetite control.

59

60 **RESULTS**

61 ***Whole brain activity mapping of appetite-regulating regions***

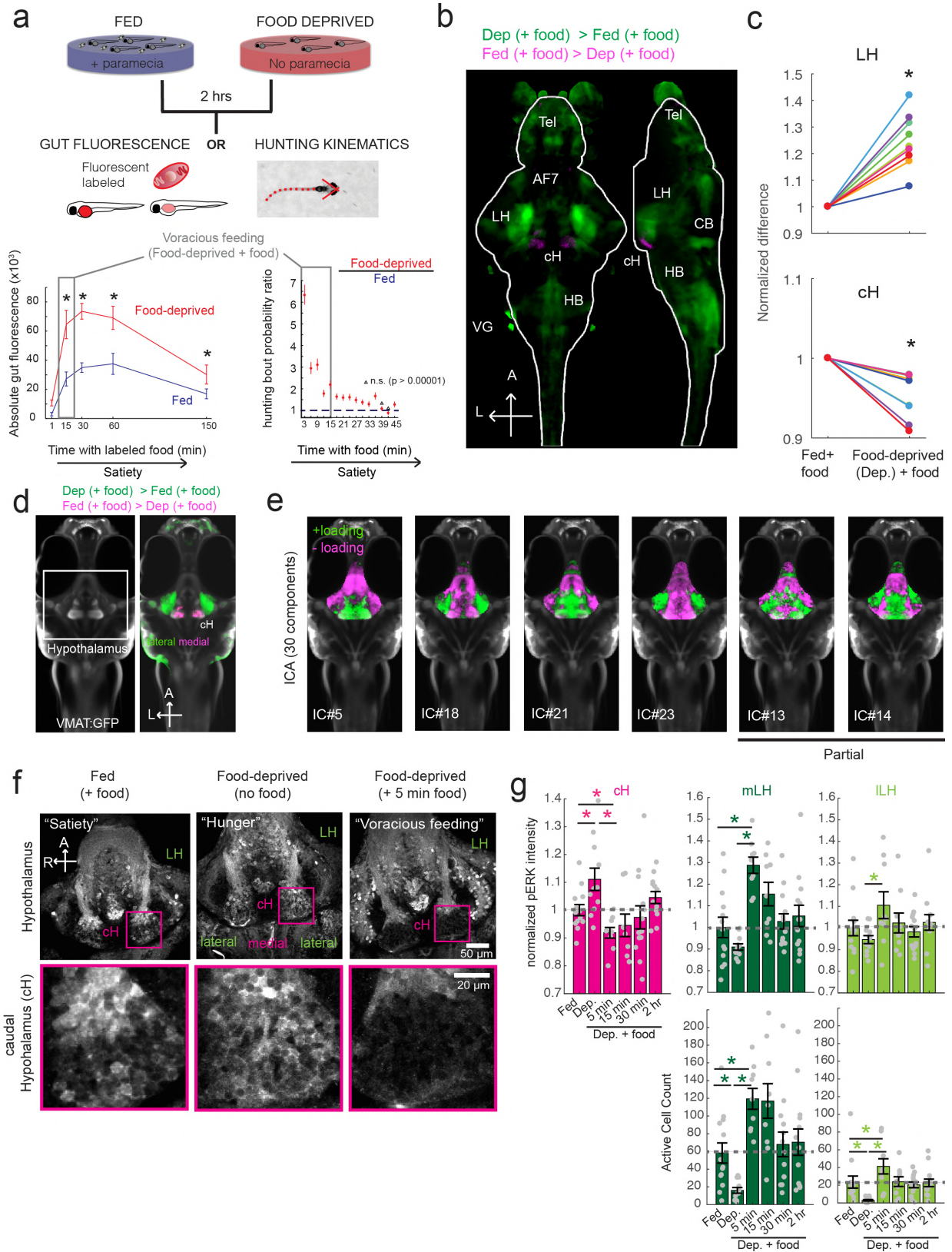
62 Larval zebrafish hunt their prey, paramecia, through a sequence of motor actions that has been
63 considered a hardwired reflex response to external prey stimuli (Bianco et al., 2011;
64 Semmelhack et al., 2015; Trivedi and Bollmann, 2013). Only recently has evidence emerged
65 that this behavior is flexibly modulated by satiation state (Filosa et al., 2016; Jordi et al., 2015,
66 2018) and that larvae at 7 days post-fertilization (dpf) display enhanced hunting and enhanced
67 food intake after a period of food deprivation. A robust readout of food intake in larval zebrafish
68 was obtained both by fluorescently-labeled paramecia and behavioral analysis approaches that
69 have been adapted for this study (Jordi et al., 2015, 2018; Shimada et al., 2012, Johnson et al.,
70 in preparation, Figure 1a). Given that a 2-hour period of food-deprivation is sufficient to robustly
71 enhance subsequent food intake, fish at the end of this food-deprivation period are considered
72 to be in a state of “hunger” and nutrient/caloric deficit. Indeed, up to 15 min after food-
73 presentation, such food-deprived animals display a strong upregulation of hunting and food
74 intake relative to fish with continuous access to food (fed fish). As the fish in this state are likely
75 still in a caloric/nutrient deficit and display enhanced food intake, we will refer to this phase as
76 “voracious feeding”. Finally, as the fish continue to consume food, their rate of food intake
77 declines to a low level comparable to that of fed fish. As we describe below, this state of
78 continuous low level feeding in the presence of ample food sources reflects a state of “satiety”

79 that is the same or similar to that of a continuously fed animal.

80 As a first step toward understanding the homeostatic control of feeding in this simple
81 vertebrate system, we employed whole-brain neuronal activity mapping via phosphorylated ERK
82 visualization in post-fixed animals (MAP-mapping; Randlett et al., 2015). Whole brain confocal
83 image datasets of phospho-ERK expression were gathered from animals sacrificed after 15
84 minutes of voracious feeding that followed a 2-hour period of food deprivation. For comparison,
85 image sets were also gathered from animals that had been fed constantly. These image
86 volumes were registered to a standardized brain atlas and are displayed as a difference map
87 (Figure 1b), revealing significant differences in neural activity when comparing voracious
88 feeding with constant feeding (Figure 1b-d, Video 1, Supplementary Tables 1-2). Since both
89 experimental groups experienced similar sensory stimuli (i.e. exposure to the same
90 concentration of paramecia), differences in brain activity should reflect the animal's internal
91 hunger state, which could also manifest as an enhanced sensitivity to food cues, and/or
92 enhanced hunting and prey capture. Indeed, multiple sensorimotor loci related to hunting
93 showed enhanced activity in the food-deprived state. These included stronger activation in
94 retinal Arborization Fields (AFs; optic tectum and AF7), pretectum, as well as downstream
95 hindbrain loci, such as reticulospinal and oculomotor neurons that all have been shown to be
96 engaged during prey capture behavior (Bianco and Engert, 2015; Muto et al., 2017;
97 Semmelhack et al., 2015). In addition, enhanced activity was observed in the cerebellum,
98 inferior olive, vagal sensory and motor neurons, area postrema and locus coeruleus, all of which
99 have been implicated in producing motor programs related to feeding behavior (Ahima and
100 Antwi, 2008; Ammar et al., 2001; Dockray, 2009; Zhu and Wang, 2008).

101 We next focused our attention on brain areas likely to be involved in regulating internal
102 states related to hunger and satiety. These included an area of particularly strong differential
103 activity in the lateral region of the intermediate hypothalamus (LH; Fig. 1b-d), which has recently
104 been identified as part of the feeding pathway in larval zebrafish (Muto et al., 2017), and whose

105 mammalian analog has been strongly implicated in appetite control (Sternson and Eiselt, 2017).
106 However, the zebrafish LH, unlike its mammalian counterpart, does not express melanin-
107 concentrating hormone (MCH) or contain orexin (hypocretin)-positive neurons, nor does it
108 clearly express other major feeding-related peptides (Figure 1- Figure Supplement 1 and 2).
109 MCH, hypocretin and other appetite-related neuromodulators (AgRP, MSH, CART, NPY) are in
110 fact expressed in other nearby areas of the hypothalamus (Figure 1 - Figure Supplement 1).
111 The zebrafish LH region does however contain a variety of glutamatergic and GABAergic cell
112 types (Figure 1 - Figure Supplement 2) that have been shown to be important for regulation of
113 feeding in mammals, independent of MCH and orexin (Jennings et al., 2015; Stuber and Wise,
114 2016). Among areas that showed relatively decreased neural activity upon feeding food-
115 deprived animals, the most significant was the caudal hypothalamus (cH), which contains
116 monoaminergic (mainly serotonergic and dopaminergic) neurons (Fig 1c; Kaslin and Panula,
117 2001; Lillesaar, 2011). Indeed, in all of nine independent MAP-mapping experiments, activity
118 was reduced in the cH and increased in the LH within 15 min of food presentation (Fig 1c). The
119 evident inverse relationship between overall LH and cH activity in this context was supported by
120 independent component analysis (Randlett et al., 2015), which was applied to all feeding-related
121 MAP-mapping data, and uncovered multiple components where the cH and LH are strongly
122 anti-correlated (Figure 1e, Figure 1 - Figure Supplement 3). These results led us to hypothesize
123 that the lateral and caudal hypothalamus may form a functionally interconnected network with
124 opposing activity patterns.



125
126
127
128

Figure 1 with 4 supplements: Whole brain activity mapping reveals anti-correlated hypothalamic clusters

129 **(a)** Top: Schematic of protocols used to evaluate appetite behavior in larval zebrafish. At 7 or 8 dpf,
130 larvae were either food-deprived for 2 hours, or fed with excess paramecia for this duration. After 2 hrs (2-
131 4 hours in the case of behavioral imaging), they were subject to a quick wash, followed either by: 1)
132 addition of excess fluorescent-labeled paramecia (left), 2) high-resolution behavioral imaging (right).
133 **Bottom left:** Gut fluorescence measurements of food-deprived (red) or fed (blue) fish as a function of
134 feeding duration. Groups of fed or food-deprived larvae were fixed at indicated time points after feeding of
135 labeled paramecia (fed: n=7/18/19/17/17, food-deprived: n= 8/23/20/14/15). Food-deprived fish had
136 significantly higher gut fluorescence than fed fish overall ($p = 7.5859 \times 10^{-10}$, Two-way ANOVA, asterisk
137 indicates corrected p-values < 0.05. **Bottom right:** The probability of performing a hunting-related swim
138 bout across fed and food-deprived fish groups in 3-minute time bins over 45 minutes. Error bars represent
139 90% confidence intervals. For all bins except those indicated with triangles, the null hypothesis that initial
140 feeding condition has no effect on hunting-bout probability is rejected ($p < 0.00001$, Fisher's Exact Test
141 comparing binomial probability distributions per bin). Fed: n = 85655 bouts from 73 fish; Food-deprived n =
142 75357 bouts from 57 fish. Since the rate of food intake and hunting behavior was highest in the first 15
143 minutes (voracious feeding phase, gray boxes), we chose this time point for subsequent MAP-mapping
144 experiments.

145 **(b)** Brain-wide activity mapping of food-deprived (Dep.) and fed fish, in response to food. Data from 9
146 experiments (n = 557 fish total) were combined to generate this map. Activated regions include the
147 telencephalon (Tel), Arborization field 7 (AF7), cerebellum (CB), hindbrain (HB), Vagal ganglion (VG) and
148 lateral lobe of the intermediate hypothalamus (LH). Suppression was observed in the caudal
149 hypothalamus (cH) and some parts of the telencephalon. Scale bar = 100 μm . Also see Video 1.

150 **(c)** ROI-specific analysis of LH and cH regions in 9 independent MAP-mapping experiments (20-30 fish
151 per treatment per experiment). Food-deprived fish constantly had higher LH and lower cH activity in
152 response to food ($p=0.0039$ for both cH and LH, Wilcoxon Signed Rank Test).

153 **(d)** Z-projection of same MAP-map showing the hypothalamus, where lateral regions (i.e. LH) are strongly
154 activated and medial regions (e.g. cH) are suppressed. The map is overlaid on an anatomy stack for the
155 transgenic line *Tg(etVMAT:GFP)* to highlight the location of cH neurons.

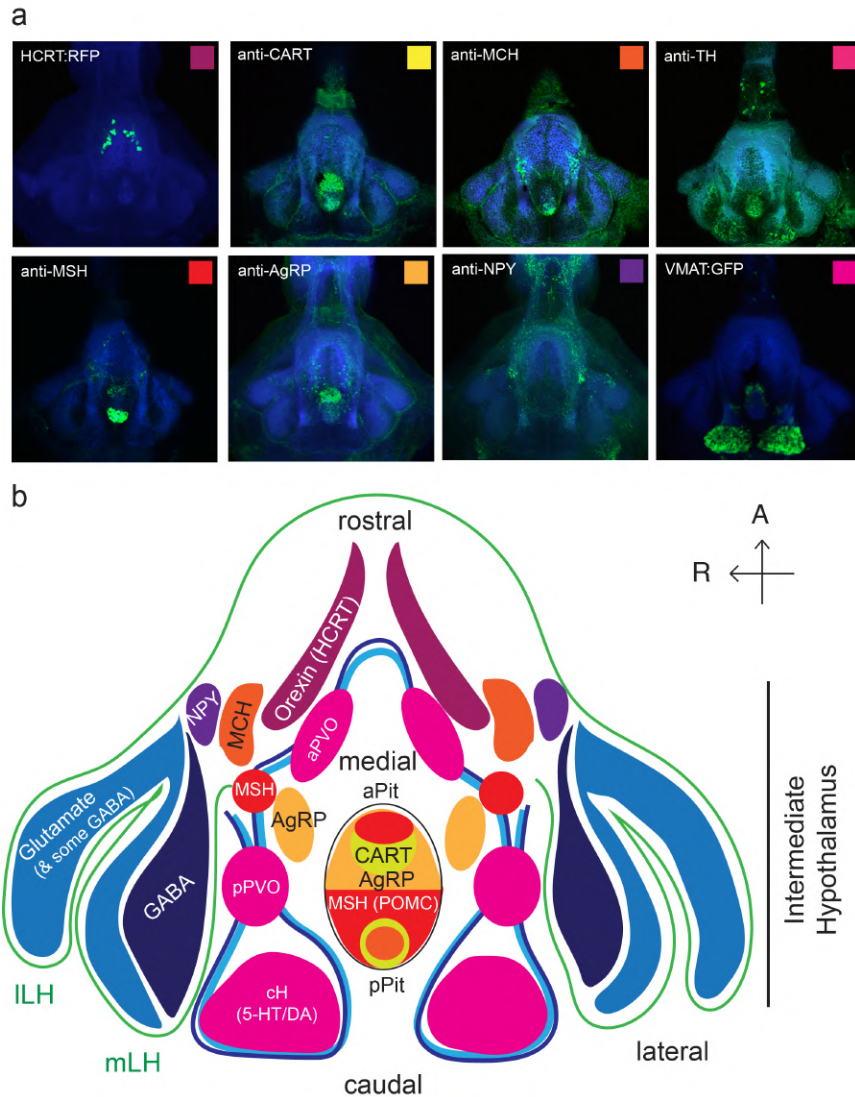
156 **(e)** Six examples of independent component analysis (ICA) maps. Voxels for each recovered independent
157 component (IC) are shown as maximum projections, with intensity proportional to the z-score of the
158 loadings of the ICA signal. These ICs, along with others (16/30) highlight LH and cH regions of opposite
159 loadings, suggesting they may be part of a network with anti-correlated activity patterns. Positive (+)
160 loading and Negative (-ve) loadings are reflected in green and magenta respectively.

161 **(f)** Higher resolution imaging of dissected brains stained with pERK during phases of feeding. Scale bar:
162 50 μm . Inset: Higher magnification view of cH neurons. Scale bar: Scale bar = 20 μm . Fish were mounted
163 ventral side up.

164 **(g)** Quantification of cH activity (normalized pERK fluorescence) and LH (medial LH and lateral LH)
165 activity (normalized pERK fluorescence) (top) and # pERK-positive cells (bottom) in fed and food-
166 deprived fish (n = 13/11/9/9/13/12).

167 Normalized pERK intensity (cH/mLH/ILH): Fed vs Dep. ($p = 0.016/0.17/0.17$), Dep. vs Dep + 5 min food
168 ($p=3.1 \times 10^{-4}/9.9 \times 10^{-5}/0.02$), Fed vs Dep. + 5 min food ($p= 0.0097/0.001/0.08$).

169 Active Cell count (mLH/ILH): Fed vs Dep. ($p = 0.001/0.0038$), Dep. vs Dep + 5 min food ($p= 9.7 \times 10^{-5}/1.3 \times 10^{-5}$), Fed vs Dep. + 5 min food ($p= 0.0038/0.048$). Asterisks denote $p < 0.05$, one-tail Wilcoxon
170 Rank Sum Test. Note that mean pERK intensity does not change as significantly as active cell count.
171



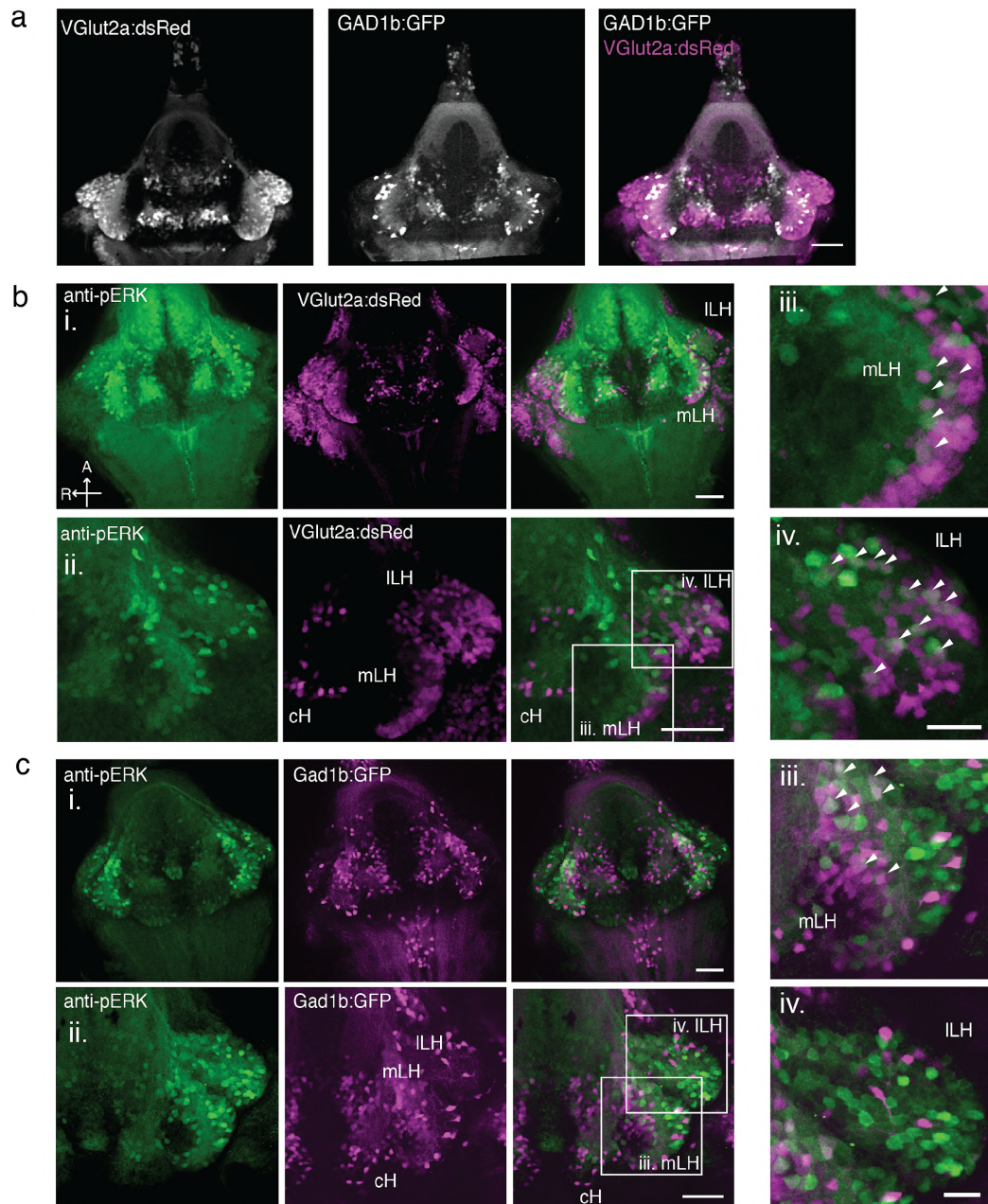
172
173

174 **Figure 1 - Figure Supplement 1: Anatomical characterization of intermediate hypothalamus**
175 **feeding areas**

176 **(a)** Expression patterns of a number of feeding-related peptides in the zebrafish hypothalamus, based on
177 antibody-staining or transgenic labels. HCRT = hypocretin (orexin), CART = cocaine and amphetamine
178 related transcript MCH = melanin-concentrating hormone, TH = tyrosine hydroxylase (labels
179 dopaminergic and/or noradrenergic neurons), MSH = alpha-melanocyte stimulating hormone, AgRP =
180 Agouti-related peptide, NPY = neuropeptide Y, VMAT = vesicular monoamine transporter (labels
181 dopaminergic (DA) and serotonergic neurons (5-HT)). Note that MCH and HCRT staining is absent from
182 the zebrafish LH. Though not apparent from the schematic, HCRT is located more dorsally. The preoptic
183 area, which contains oxytocinergic as well as other peptidergic neurons, is located more dorsally and not
184 reflected in this schematic.

185 **(b)** Schematic summarizing zebrafish hypothalamic peptide expression. GABA (dark blue) and
186 glutamatergic (blue) neurons are found in the lateral hypothalamus (see Figure 1- Figure Supplement 2)
187 and also throughout the medial regions of the hypothalamus. PVO = paraventricular organ, which also
188 contains DA and 5-HT neurons. A number of peptidergic neurons are located within the anterior and
189 posterior pituitary/hypophysis (aPit and pPit). Color code corresponds to images in (a).

190



191

192

Figure 1- Figure Supplement 2: Characterization of zebrafish LH

193

(a) Glutamatergic and GABAergic neuron distribution in the hypothalamus. *Tg(VGlut2a:dsRed)* and *Tg(GAD1b:GFP)* transgenic fish were dissected, imaged and registered onto a common reference hypothalamus.

196

(b) Glutamatergic cells, labeled by *Tg(VGlut2a:dsRed)*, overlap with active (pERK-positive) neurons in both the ILH and outer rim of the mLH. (i) Overview of hypothalamus. (ii) Higher magnification images of LH. (iii-iv) Inset showing overlap of ILH and outer rim of mLH with glutamatergic cells.

199

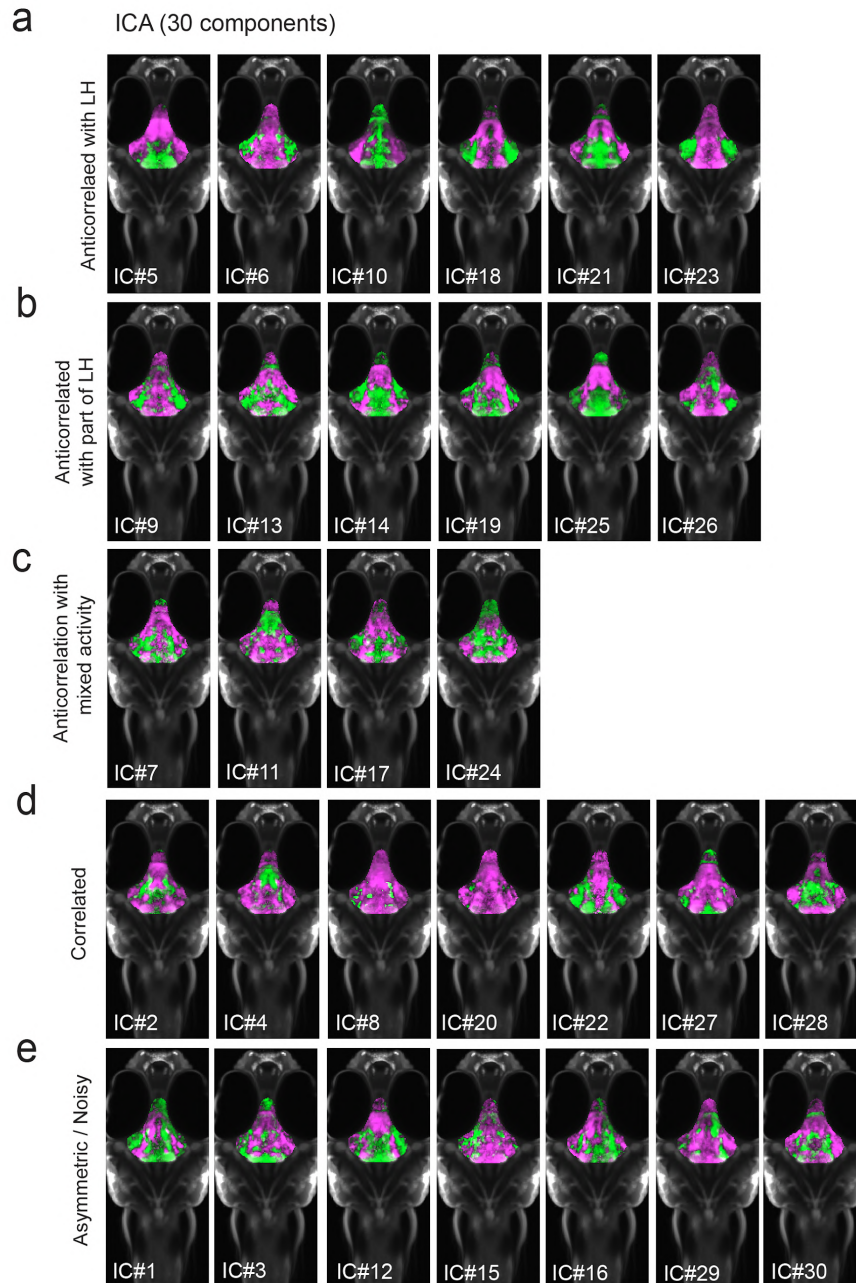
(c) GABAergic cells, labeled by *Tg(Gad1b:GFP)*, overlap with active neurons in the inner rim of the mLH but not the ILH. (i) Overview of hypothalamus. (ii) Higher magnification images of LH. (iii-iv) Inset showing overlap of inner rim of mLH with GABAergic cells. White arrows point to examples of overlapping cells.

200

All fish were mounted ventral side up. Scale bar = 50 µm. Inset scale bar = 20 µm.

201

202



203

204

Figure 1- Figure Supplement 3: All 30 independent components extracted from ICA analysis. This

method separates pERK signals into statistically independent components based on their correlated

activity, thus identifying putative functional connectivity (both positive or negative relationships) between

different brain regions (Randlett et al., 2015; see Methods). To increase the robustness of the analysis,

we included fish from other feeding-related treatments that we did not otherwise use in this manuscript (n

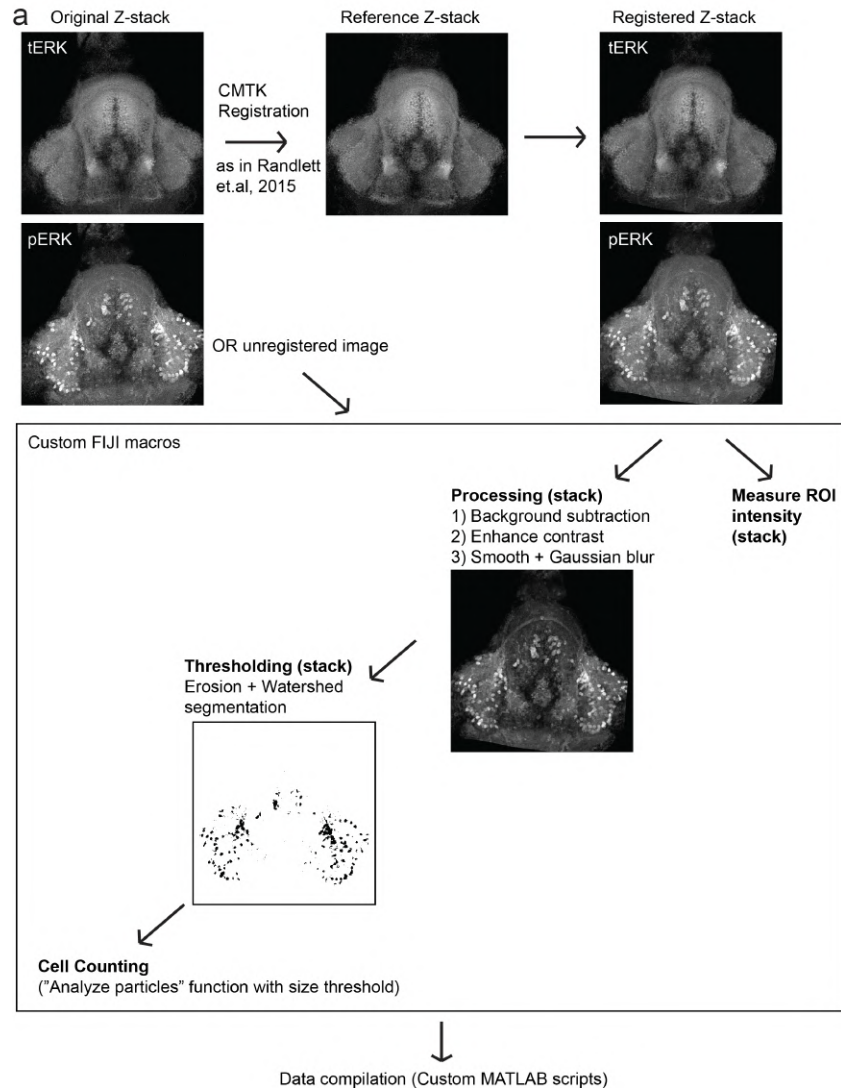
= 904 fish total).

(a-c) From this analysis, we identified multiple independent component networks (ICs) in which at least

part of the LH displayed an inverse activity relationship (i.e. opposite loadings) with the cH (16/30).

(d) 7/30 ICs had correlated LH and cH activity.

(e) The other 7/30 had asymmetrical or noisy activity patterns.



214

215 **Figure 1 – Figure supplement 4: Automated quantification of pERK-positive cells**

216 **(a)** Method by which we quantify pERK-positive ("active") cell count in a high-throughput manner. This
217 method works best with high-resolution images (i.e. dissected brains). Brain stacks are registered onto a
218 reference brain within the same dataset, using the tERK channel, though there is the option of using
219 unregistered images (for which individual ROIs have to be defined for each image). A series of
220 processing steps allows for automated segmentation of pERK-positive cells using the same manually
221 optimized threshold across the entire dataset.

222

223 **Cellular dissection of hypothalamus neural activity reveals modulation by satiation state**

224 To probe neural activity changes with higher resolution, we performed pERK staining in

225 dissected brains, and examined the activity of these populations in time course experiments that

226 spanned the period of food-deprivation and subsequent feeding (Figure 1f-g, Figure 2). We

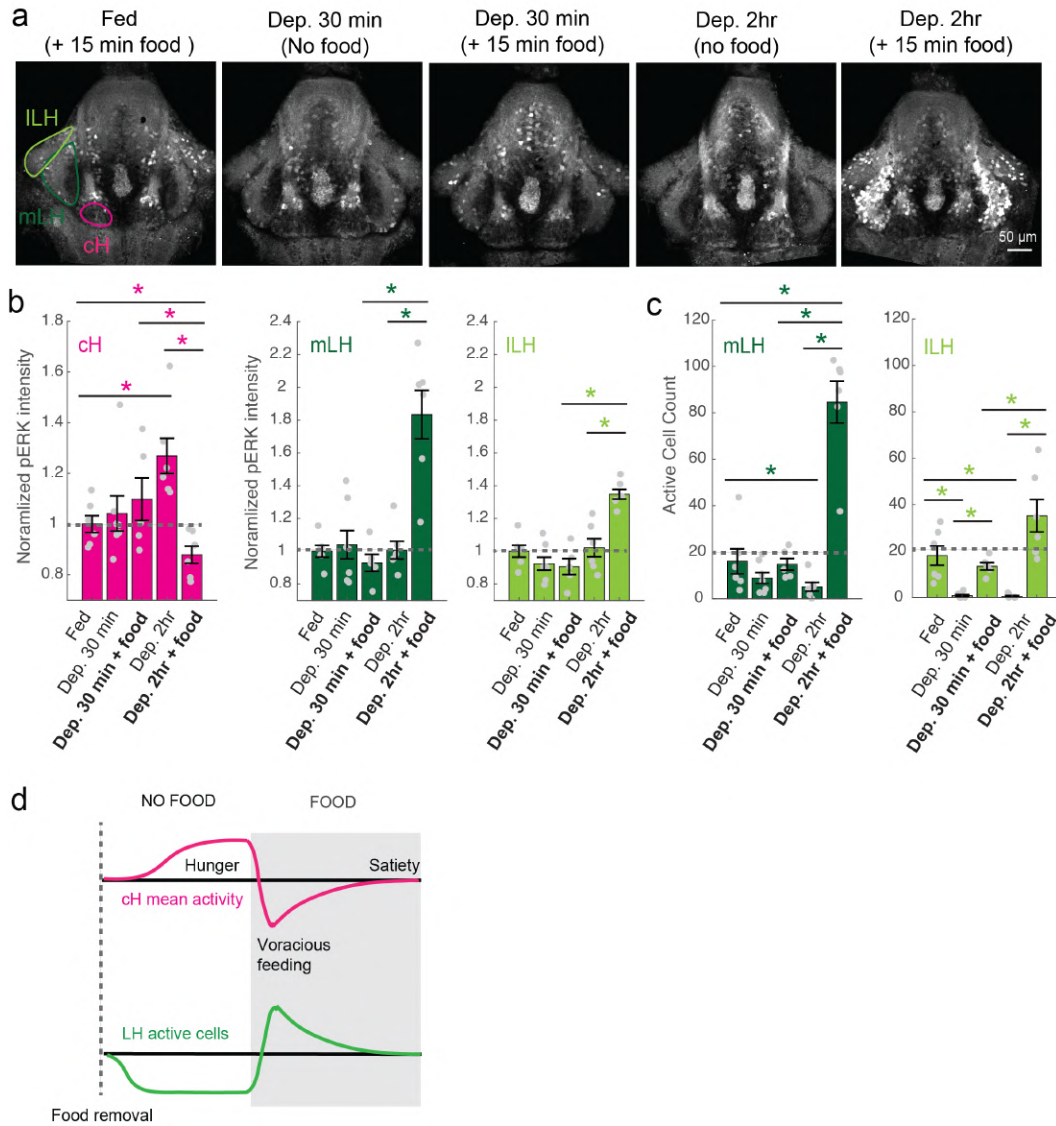
227 quantified changes in mean cellular fluorescence as well as changes in the number of active
228 cells or cell clusters (Figure 1 - Figure Supplement 4). While the high density of labeled cells
229 and high background fluorescence in the cH made the identification of individual neurons
230 difficult, we found that in the LH segmentation of individual neurons and classifying activity
231 based on the thresholded fluorescence levels provided a cleaner and more reliable readout for
232 overall neuronal activity. Using these respective metrics, we observed that mean fluorescence
233 in the cH was predictably high in food-deprived fish, while the number of active neurons in the
234 medial and lateral lobes of the LH (mLH and ILH, respectively) was low when compared to
235 continuously fed animals. However, within 5 minutes of food presentation, cH activity fell
236 dramatically to a level significantly below that observed in continuously fed fish (Figure 1f). This
237 characteristically low cH activity level was accompanied by a large increase in LH mean
238 fluorescence and neuron activity, which is consistent with our MAP-mapping results. As the
239 feeding period continued, LH neuronal activity declined and, reciprocally, cH activity increased,
240 coincident with the decline in voracious hunting and food ingestion (Figure 1f). After two hours,
241 neural activity in the cH and LH and feeding behavior all converged onto baseline levels similar
242 to those observed in continuously fed fish (Figure 1f). Thus these two neuronal populations
243 display anti-correlated activity patterns over time frames that span the progression of hunger
244 during food-deprivation, voracious feeding and the gradual return to satiety.

245 ***Satiation state influences the sensitivity of cH and LH populations to food***

246 The neural activity patterns described above suggest that cH and LH activity may report the
247 satiation state of the animal. To better align these patterns with the animal's internal state, we
248 examined these loci over a time course that started with food removal from well-fed animals,
249 followed by food presentation after a variable food-deprivation period (30 min or 2 hours, Figure
250 2). We found that food removal resulted in a reduction of the number of active mLH and ILH
251 neurons within 30 minutes. In contrast, cH activity gradually increased, with a significantly
252 higher level of activity occurring between 30 min and 2 hours post-food removal. A possible

253 interpretation of these patterns is that LH activity is directly driven by the presence of food cues
254 (as noted by Muto et al 2017), whereas the level of activity observed in cH neurons is a
255 correlate of the animal's nutrient/caloric deficit and resulting hunger state in the absence of food,
256 possibly even generating the signal necessary to sensitize the LH's responsiveness to such
257 stimuli.

258 Food presentation not only rapidly reverses the activity patterns of both loci, but also
259 does so in a manner correlating with the length of food-deprivation. Indeed, fish that had been
260 food-deprived for longer periods (2-4 hrs) displayed a relatively enhanced induction of LH
261 activity upon the introduction of food. Likewise, the reduction in cH activity on food presentation
262 was significantly more pronounced when it followed a longer period of prior deprivation; both of
263 these neural responses were strongly correlated with enhanced food consumption (voracious
264 feeding; Figure 2, Figure 2 – Figure Supplement 1). As prey continues to be consumed, activity
265 in both loci gradually reverts back to the baseline levels representative for fed animals (Figure
266 1f-g, 2d).



267

268

Figure 2 with 5 supplements: cH and LH activities are modulated by food and satiation state

269

(a) Representative images showing how cH and LH activity in the presence and absence of food vary with the extent of food-deprivation, from the same dataset quantified below.

270

(b) Mean pERK fluorescence in the cH increases with food-deprivation, whereas mean LH pERK fluorescence does not change significantly, except during voracious feeding (Dep. 2hr + food).

271

Normalized pERK intensity (cH/mLH/ILH): Fed vs Dep. 2hr ($p = 0.0022/0.41/0.59$), Fed vs Dep. 2hr +

272

food ($0.047/0.0011/0.0011$), Dep. 30 min + food vs Dep. 2hr + food ($p = 0.041/0.0022/0.0022$), Dep. 2hr

273

vs Dep. 2hr + food ($p = 0.0022/0.0011/0.0022$).

274

(c) The number of active LH (particularly ILH) cells decline within 30 min of food deprivation, and is

275

significantly enhanced during feeding, particularly after a longer period of food-deprivation. Active cell

276

count (mLH/ILH): Fed vs Dep. 30 min ($p = 0.155/5.8 \times 10^{-4}$), Fed vs Dep. 2hr ($p = 0.047/0.011$), Dep. 30

277

min + food vs Dep. 2hr + food ($p = 0.0022/0.0043$), Dep. 30 min vs Dep. 30 min + food ($p = 0.07/0.013$),

278

Dep. 2hr vs Dep. 2hr + food ($p = 0.0011/0.0011$), Fed vs Dep. 2hr + food ($p = 0.0022/0.07$), $n = 6/7/5/6/6$

279

fish, One-tail Wilcoxon Rank Sum Test.

280

(d) Schematic of inferred cH and LH activity over phases of feeding. LH active cell count appears to

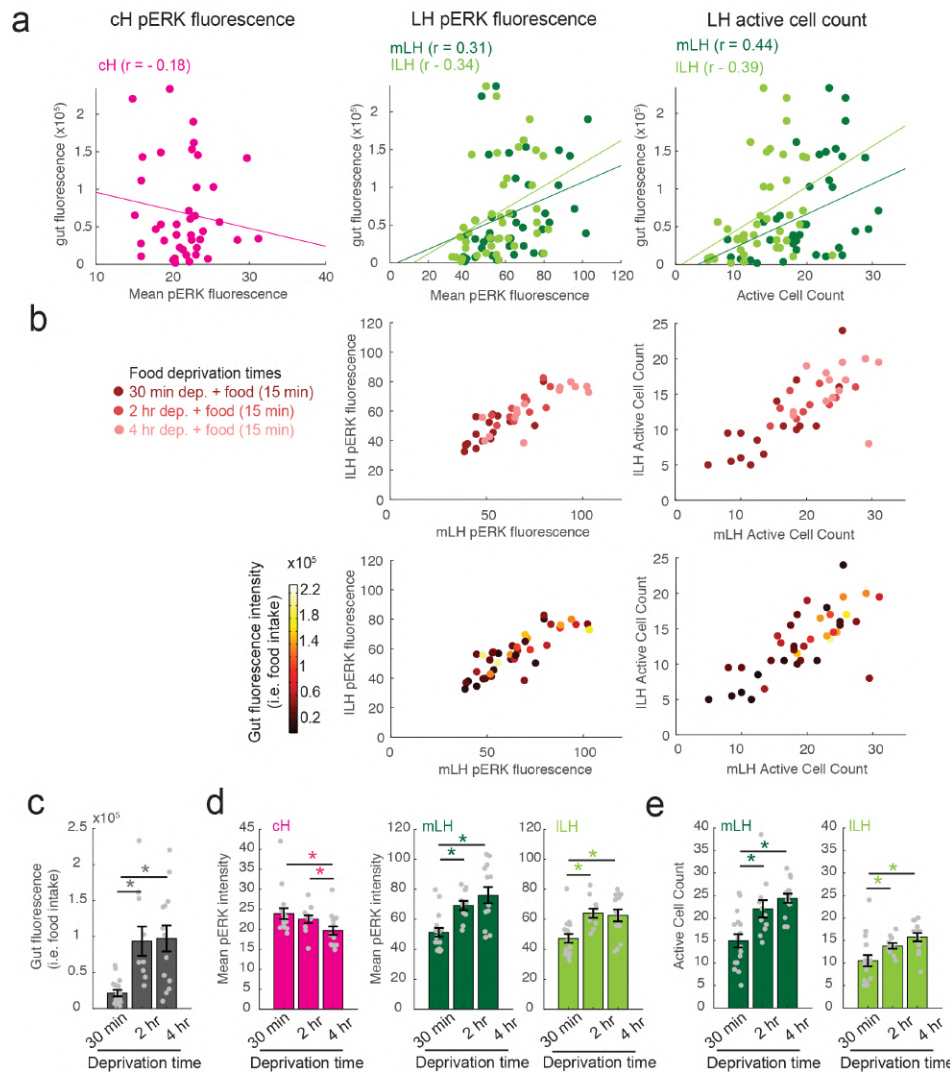
281

decline more rapidly than the rise in cH activity. More supporting data can be found in the supplements.

282

283

284



285

286

287

Figure 2 - Figure Supplement 1: Additional data showing modulation of cH and LH by satiation state, and correlation with food intake

288

(a) Gut fluorescence (i.e. food intake) as a function of mean cH pERK fluorescence, mean LH (mLH and ILH) pERK fluorescence and active cell count.

289

(b) Top: mLH and ILH mean pERK fluorescence (left) and active cell count (right) as a function of food-deprivation time (denoted by color intensity). **Bottom:** mLH and ILH mean fluorescence (left) and cell count (right) as a function of gut fluorescence (i.e. food intake) after 15 min of feeding (denoted by color intensity).

290

(c-e) Quantification of gut fluorescence, cH and LH mean pERK fluorescence and LH active cell count across different food deprivation times (30 min, 2hr and 4hr). Note that in this dataset, these fish brains have been stained individually, which may have affected cH quantification.

291

(c) Food intake: 30 min vs 2hr dep. ($p = 2.8 \times 10^{-4}$), 30 min vs 4hr dep. ($p = 4.0 \times 10^{-4}$), 2hr vs 4hr dep. ($p = 0.56$). Asterisk denotes $p < 0.05$, $n = 16/11/14$ fish, One-tail Wilcoxon Rank Sum Test.

292

(d) Mean pERK fluorescence (cH/mLH/ILH): 30 min vs 2hr dep. ($p = 0.60/0.001/5.9 \times 10^{-4}$), 30 min vs 4hr dep. ($p = 0.084/8.6 \times 10^{-4}/0.058$), 2hr vs 4hr dep. ($p = 0.02/0.24/0.54$)

293

(e) Active cell count (mLH/ILH): 30 min vs 2hr dep. ($p = 0.0073/0.0094$), 30 min vs 4hr dep. ($p = 1.6 \times 10^{-4}/0.0017$), 2hr vs 4hr dep. ($p = 0.056/0.053$).

294

295

296

297

298

299

300

301

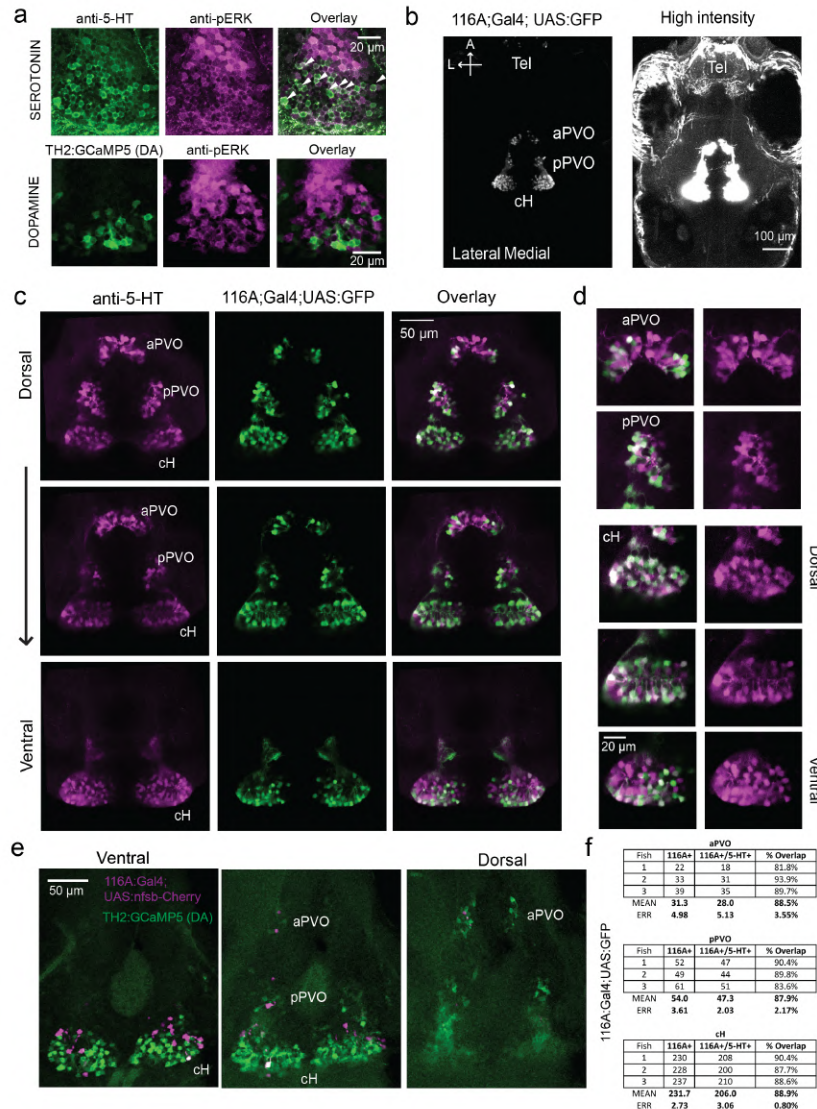
302

303

304 Given the indirect nature of activity mapping in post-fixed animals, as above, we
305 employed *in vivo* calcium imaging to measure cH and LH neuronal activities during food
306 deprivation in real time (Figure 2 - Figure Supplement 3-5). Two transgenic Gal4 drivers,
307 *Tg(116A:Gal4)* and *Tg(76A:Gal4)*, were used to drive expression of GCaMP6s
308 (*Tg(UAS:GCaMP6s)*) in large subsets of cH and LH neurons (Figure 2 - Figure Supplement 2-
309 3). The 116A:Gal4 transgene drives expression mainly in serotonergic neurons in the cH
310 ($88.9\pm 0.8\%$ 5-HT positive) and paraventricular organ (PVO; Figure 2- Figure Supplement 2),
311 whereas 76A:Gal4 drives expression in a large proportion of LH cells (Figure 2 - Figure
312 Supplement 3, Muto et al., 2017). Consistent with our pERK results, the initial calcium-mediated
313 mean fluorescence and firing frequency of a subset of cH neurons scaled with the length of
314 food-deprivation prior to imaging (Figure 2- Figure Supplement 3d), and increased further as
315 food-deprivation continued over the 2 hr imaging period (Figure 2 - Figure Supplement 3-5).
316 The largest rate of increase occurred during the initial hour of food-deprivation (Figure 2 - Figure
317 Supplement 3-5).

318 Analysis of LH activity gave more diverse results over the course of the food-deprivation
319 time course. While some mLH and ILH voxels showed a predicted reduction in baseline
320 fluorescence and firing rate, many others displayed a significant enhancement of baseline
321 activity. It is possible that these changes reflect real dynamics in certain cellular or neuropil
322 subtypes within the LH, or that they are artifacts of head fixation. Despite the significant diversity
323 in response properties within the LH, we still observe, in line with our expectations, an overall
324 negative correlation of ILH calcium spikes with the mean value of cH fluorescence (Figure 2 -
325 Figure Supplement 4 and 5).

326
327



328
329
330
331
332
333
334
335
336
337
338
339
340
341
342
343
344

Figure 2 - Figure Supplement 2: Characterization of the cH and 116A:Gal4 line

(a) pERK-positive cH cells overlaps with anti-5-HT immunostaining and *Tg(116A:Gal4)* cells, and less with *Tg(TH2:GCaMP5)* (i.e. dopaminergic) cells. Scale bar = 20µm. White arrows point to examples of overlapping cells.

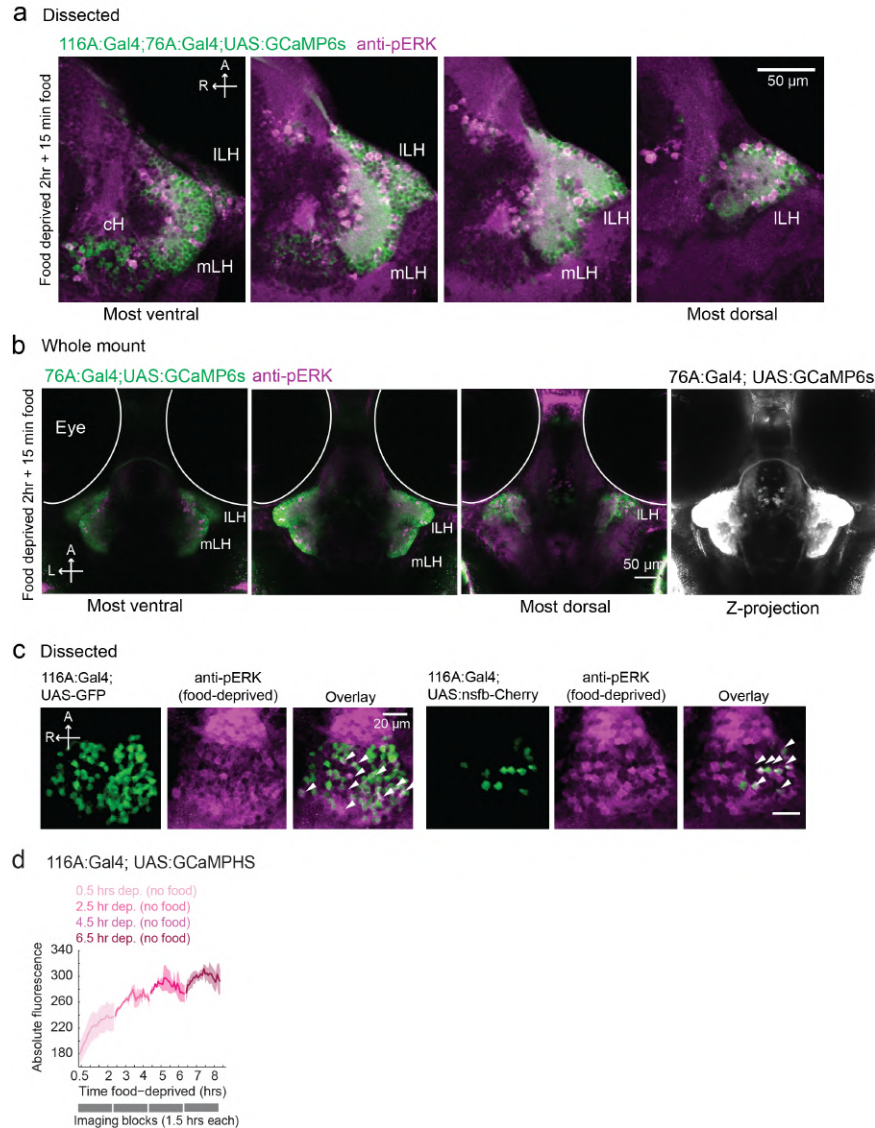
(b) Z-projection images of whole mount *Tg(116A:Gal4;UAS:GFP)* fish at low (left) and high (right) intensities. Scale bar = 100 µm.

(c) Overlap of *Tg(116A:Gal4;UAS:GFP)* with anti-5-HT immunostaining is seen in all layers of the caudal hypothalamus, and also the anterior and posterior paraventricular organ (aPVO and pPVO). Each row shows a different Z-plane, moving from more dorsal to more ventral. Scale bar = 50 µm.

(d) Higher magnification images of cH, aPVO and pPVO from left side of image in **(c)**.

(e) Minimal overlap of *Tg(116A:Gal4;UAS:nfsb-mCherry)* with dopamine neurons labeled by *Tg(TH2:GCaMP5)*. Note that the *Tg(116A:Gal4;UAS:nfsb-mCherry)* transgenic, which is used in ablation experiments, shows sparser labeling than with *Tg(UAS:GFP)*. Scale bar = 50 µm.

(f) Quantification of 5-HT overlap with *Tg(116A:Gal4;UAS:GFP)* in the cH, aPVO and pPVO.



345
 346
 347
 348
 349
 350
 351
 352
 353
 354
 355
 356
 357
 358
 359
 360

Figure 2 - Figure Supplement 3: 116A and 76A:Gal4 expression overlap with pERK activity

(a) mLH and ILH activity in voraciously-feeding fish overlaps with *Tg(76A:Gal4;UAS:GCaMP6s)* expression (dissected brains). All visible pERK-positive neurons were also co-labeled with GCaMP6s. *Tg(116A:Gal4)* is also expressed. Scale bar = 50 μ m.

(b) mLH and ILH activity in voraciously-feeding fish overlaps with *Tg(76A:Gal4;UAS:GCaMP6s)* expression (whole-mount). All visible pERK-positive neurons were also co-labeled with GFP. Note that more dorsally and anteriorly other neurons beyond the LH are labeled. Scale bar = 50 μ m.

(c) pERK positive cells (food-deprived fish) overlap partially with *Tg(116A:Gal4)* expression. Left: *Tg(116A:Gal4;UAS:GFP)* Right: *Tg(116A:Gal4;UAS:nfsb-mCherry)*. Scale bar = 20 μ m.

(d) Mean cH activity (*Tg(116A:Gal4;UAS:GCaMP6s)*) increases as a function of food-deprivation time. Larvae were food-deprived for 0.5, 2.5, 4.5 or 6.5 hours ($n = 12/4/4/8$), quickly embedded in agarose and subsequently imaged for 1.5 hours (every 5 minutes) under a confocal microscope. See Figure 2 - Figure Supplement 4-5 for simultaneous calcium imaging of cH and LH activity at higher temporal resolution.

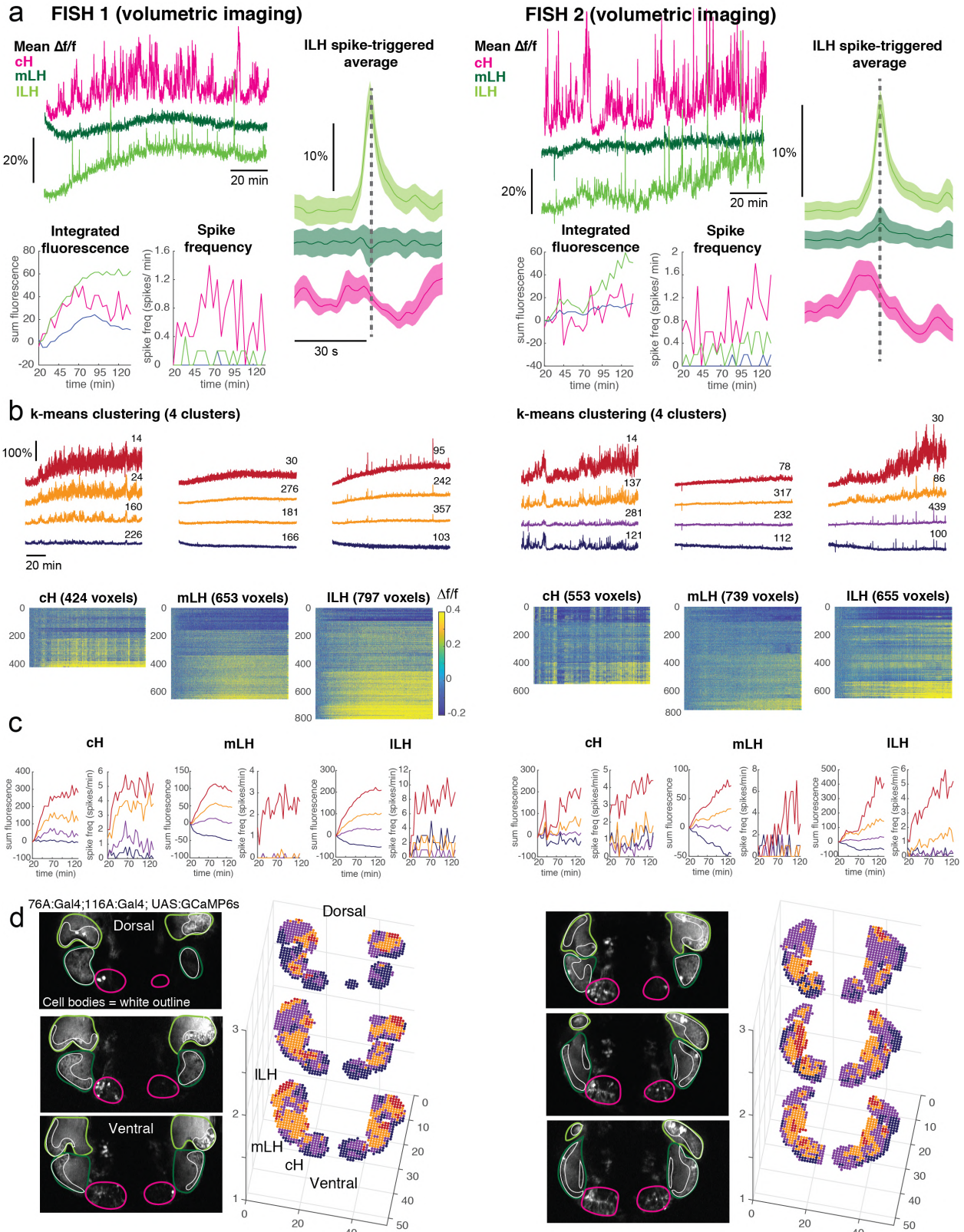
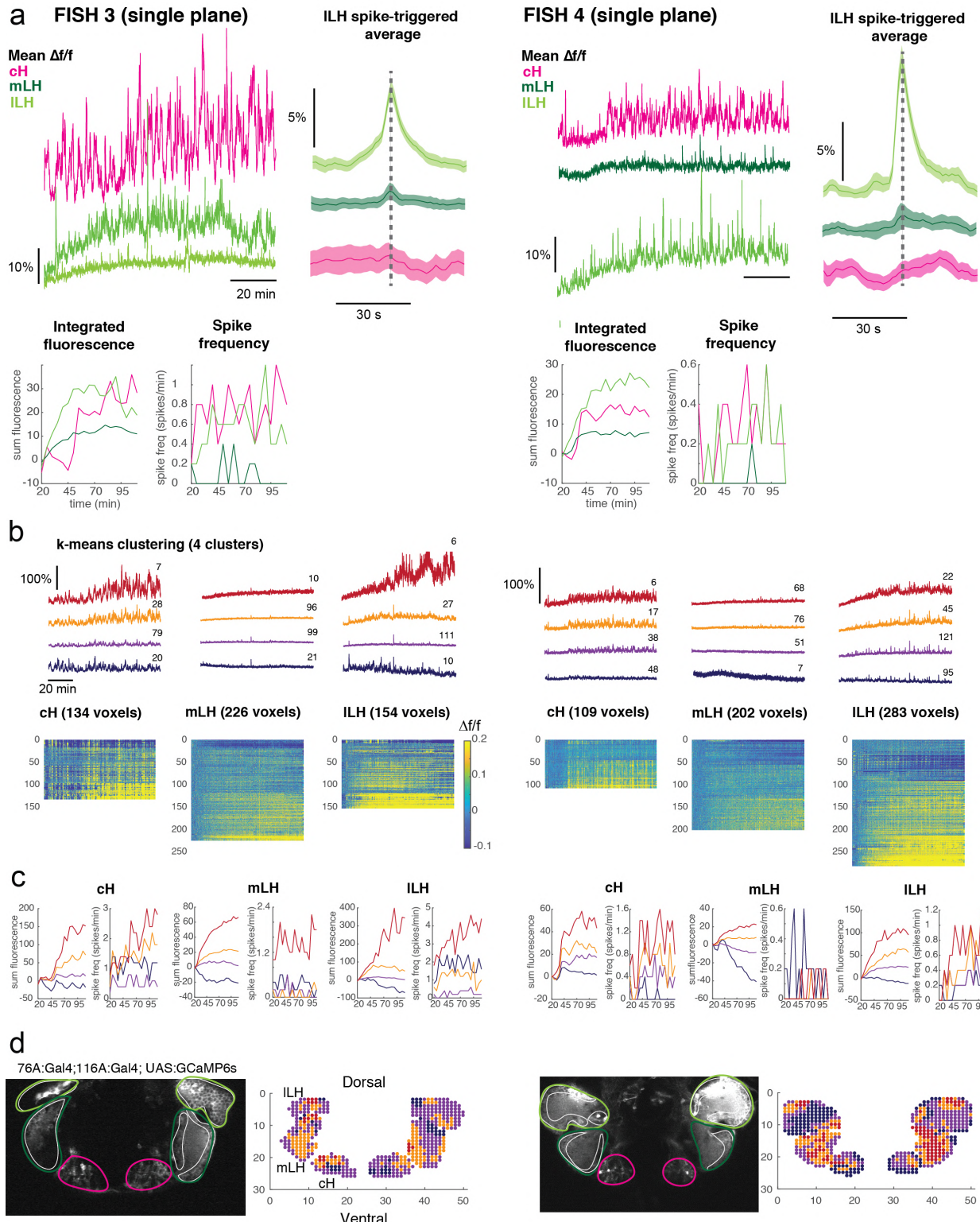


Figure 2 - Figure Supplement 4: Calcium imaging of cH and LH over food-deprivation reveal complex dynamics (volumetric imaging)

361
362
363

364 **(a)** Two fish (left and right) are shown. **Top left:** Mean $\Delta f/f$ across the entire cH, mLH and ILH **Bottom**
365 **left:** calcium dynamics (integrated (sum) fluorescence and spike frequency, 5 min bins) over the
366 course of a 2 hr long imaging session. Fish were imaged ~20 min after embedding, thus initial food-
367 deprivation time is 20 min. **Right:** Spike-triggered averages based on ILH spikes reveals an
368 accompanying reduction in cH calcium fluorescence, suggesting opposing activity patterns.
369 **(b) Top:** K-means clustering (k=4) over all cH and LH voxels reveals diverse clusters of activity.
370 Number of voxels within each cluster is indicated next to the mean $\Delta f/f$ trace. **Bottom:** Raster plots of
371 clustered neurons sorted from the least active (blue) to most active (red) cluster.
372 **(c)** Calcium dynamics (integrated fluorescence and spike frequency) for each cluster over time reveal
373 diverse activity patterns (5 min bins).
374 **(d) Left:** Average intensity projection images showing imaged regions. Cell bodies are outlined in
375 white; for the LH they tend to correspond to the edges, whereas neuropil are more concentrated in
376 the center. The cH comprises mainly cell bodies. **Right:** Positions of voxels corresponding to each
377 cluster. Fish 2 is imaged at a more ventral plane than fish 1.
378



379
380
381
382
383
384

Figure 2 - Figure Supplement 5: Calcium imaging of cH and LH over food-deprivation reveal complex dynamics (single plane)

(a) Two fish (left and right) are shown. **Top left:** Mean $\Delta f/f$ across the entire cH, mLH and ILH (top left); **Bottom left:** calcium dynamics (integrated fluorescence and spike frequency, 5 min bins) over the course of a 2hr long imaging session. Fish were imaged ~20 min after embedding, thus initial food-deprivation

385 time is 20 min. **Right:** Spike-triggered averages based on ILH spikes reveals an accompanying reduction
386 in cH calcium fluorescence. As only a single-plane was imaged, the inverse relationship between the cH
387 and LH is not as prominent.

388 **(b) Top:** K-means clustering (k=4) over all cH and LH voxels reveals diverse clusters of activity. Number
389 of voxels within each cluster is indicated next to the mean $\Delta f/f$ trace. **Bottom:** Raster plots of clustered
390 neurons sorted from the least active (blue) to most active (red) cluster.

391 **(c)** Calcium dynamics (integrated fluorescence and spike frequency) for each cluster over time reveal
392 diverse activity patterns (5 min bins).

393 **(d) Left:** Average intensity projection images showing imaged regions. Cell bodies are outlined in white;
394 for the LH they tend to correspond to the edges, whereas neuropil are more concentrated in the center.
395 The cH comprises mainly cell bodies. **Right:** Positions of voxels corresponding to each cluster. Since
396 these fish were not embedded completely symmetrically, the left and right sides of the hypothalamus are
397 at slightly different dorsal-ventral positions (right sides slightly more dorsal than left sides). Fish 3 is
398 imaged at a more ventral plane than fish 4.

399

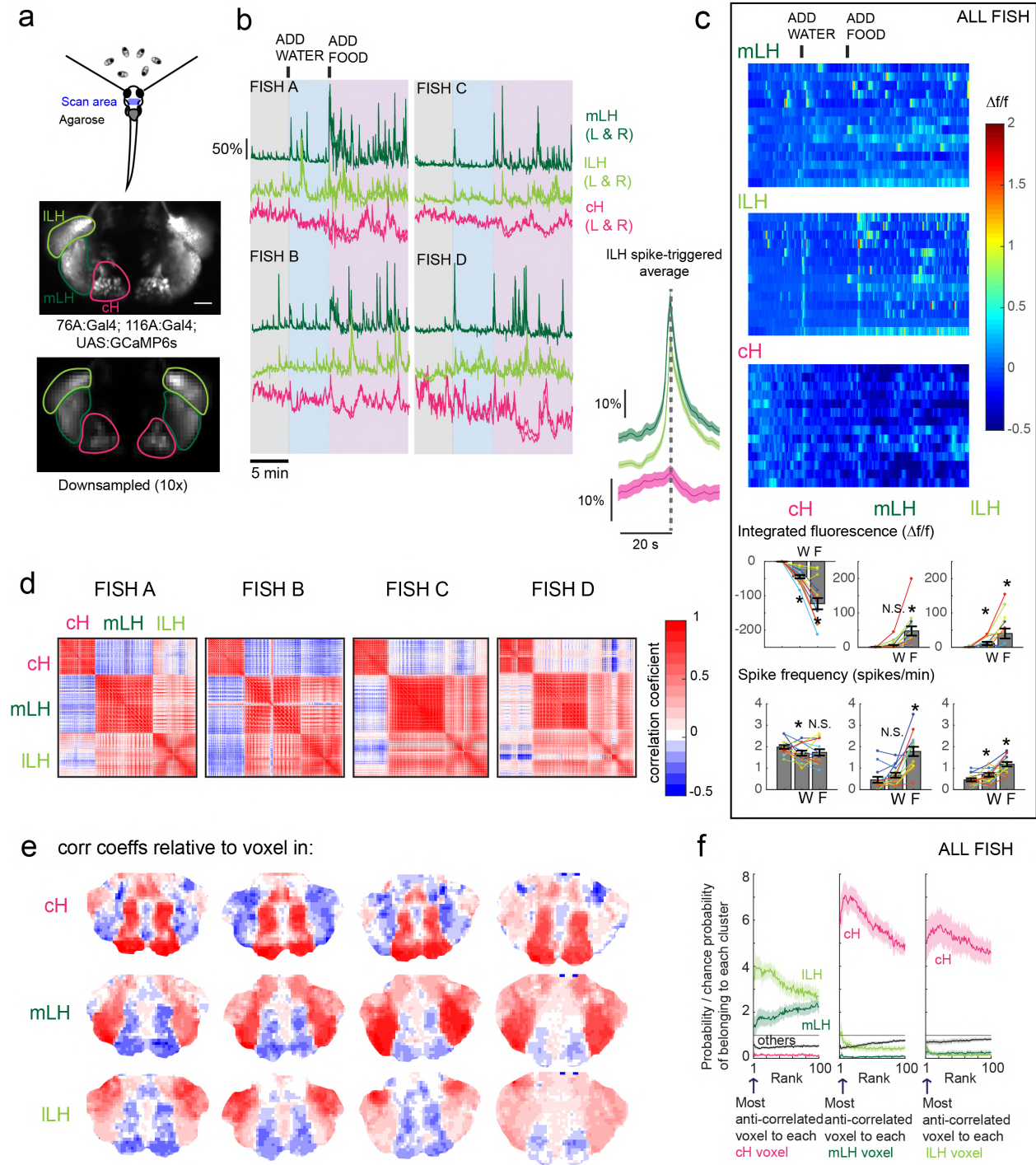
400 ***The caudal and lateral hypothalamus respond to food sensory cues and are anti-***

401 ***correlated over short timescales***

402 We next examined the effects of food sensory cues on cH and LH activity dynamics by
403 performing calcium imaging on tethered animals during the controlled presentation of food-
404 related stimuli (Figure 3a). Consistent with the above results of pERK analysis of post-fixed
405 brains, mLH and ILH neurons were strongly activated and cH neurons suppressed within
406 seconds of paramecia addition to the water in the vicinity of a food-deprived fish (Figure 3b-c).
407 Interestingly, neurons in all three hypothalamic loci responded to water flow alone (Figure 3b-c),
408 with the cH and ILH responding more strongly than the mLH (Figure 3c, bottom panels).
409 However, these responses were still significantly less than when paramecia were presented
410 (Figure 3c, bottom panels). Thus, food (and other) sensory cues in the absence of hunting or
411 food ingestion differentially modulate the activities of neurons in the caudal and lateral
412 hypothalamic lobes.

413 We also observed that, across periods in which food cues were either present or absent,
414 the activities of cH and LH neurons were remarkably anti-correlated; both spontaneous or food-
415 induced fluctuations in one population were accompanied by a corresponding opposing change
416 in the other (Figure 3b). This observation was supported by cross-correlation analysis between
417 cH, mLH and ILH voxels (Figure 3d-f), which revealed high correlation within the same

418 hypothalamic region (red), and anti-correlation between cH and LH regions (blue) (Figure 3d-e).
419 Further, ILH voxels showed more spatial heterogeneity than mLH voxels (Figure 3e), though a
420 small cluster of cells at the most-anterior part of the ILH was found to be consistently anti-
421 correlated with the cH (Figure 3e, Fish C and D, for example). When ranked according to their
422 degrees of anti-correlation with voxels from other lobes, the cH and ILH appeared to show the
423 greatest anti-correlation (Figure 3f). Overall, these results indicate that cH and LH neurons
424 display generally anti-correlated activity over short timescales in addition to longer epochs
425 reflecting states of hunger, voracious feeding and satiety.



426

427 **Figure 3: Anti-correlation on seconds timescale**

428 **(a) Top:** Schematic showing the calcium imaging setup. Transgenic fish with GCaMP-labeled cH and LH
 429 neurons were paralyzed, tethered in agarose with their eyes and nostrils freed, and exposed to live
 430 paramecia. **Top image:** GCaMP expression in the cH and LH driven by two transgenic lines. **Bottom**
 431 **image:** Downsampled image stack used for analysis
 432 **(b) Left:** Mean calcium activity from respective hypothalamic ROIs (shown in (i)) from 4 example fish after
 433 exposure to water (control) or paramecia. Left and right lobes are shown in same color and overlaid.

434 Paramecia presentation activates the LH and suppresses the cH, which show opposing activity on short
435 timescales. **Right:** Average $\Delta f/f$ triggered on ILH calcium spikes shows a mean corresponding reduction
436 in cH activity ($n = 159$ ILH spikes extracted from mean $\Delta f/f$ traces from 14 fish across the entire duration
437 of the experiment)

438 **(c) Top:** Raster plots showing mean calcium activity from the mLH, ILH and cH of 14 fish before and after
439 presentation of water and food cues. **Bottom:** Quantification of integrated (sum) $\Delta f/f$ values and spike
440 frequency (spikes/min) per fish across experimental epochs (300s baseline, 300s after water (W) delivery
441 or 600 s after food delivery (F). Water delivery was sufficient to significantly modulate both the cH (p
442 $=6.1 \times 10^{-5}$ (integrated fluorescence)/0.0497 (spike freq.) and the ILH ($p=0.029/0.026$) but not the mLH ($p =$
443 $0.48/0.055$). Note though from **(b)** that the mLH does transiently respond to water delivery. Food delivery
444 significantly increased mLH integrated fluorescence ($p=1.2 \times 10^{-4}$) and spike frequency ($p = 1.2 \times 10^{-4}$)
445 relative to water delivery. Food delivery also significantly increased ILH integrated fluorescence (p
446 $=0.045$) and spike frequency (0.0016) relative to water delivery. Food delivery significantly reduced cH
447 integrated fluorescence further relative to water delivery ($p =3.1 \times 10^{-4}$), but not spike frequency ($p = 0.52$).
448 W = water, F = food. One-tail Wilcoxon Sign Rank Test.

449 **(d)** Cross-correlogram of hypothalamic cell-sized voxels (cells and/or neuropil from downsampled image
450 stacks, see Figure 2a) from 4 example fish. cH and LH voxels were mostly anti-correlated, whereas
451 voxels within each cluster had correlated activity.

452 **(e)** Correlation coefficients of other hypothalamic voxels relative to a voxel with the cH, mLH or ILH.

453 **(f)** Summary of data from 14 fish, showing the probability of the n^{th} most anti-correlated voxel belonging to
454 each of the other clusters.

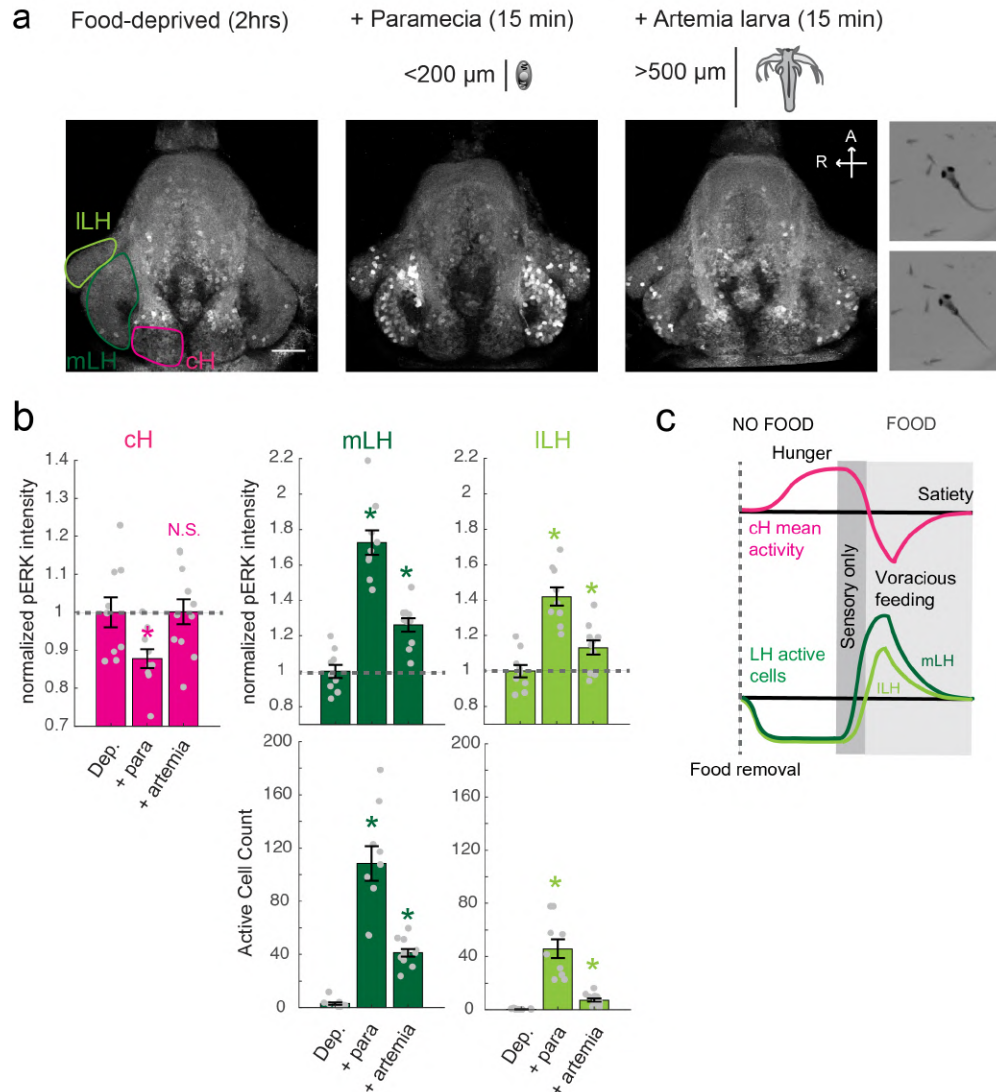
455

456 ***The activities of cH and LH neurons are differentially modulated by food sensory cues***

457 ***and ingestion***

458 We next asked whether food sensory cues might have differential and independent effects from
459 the consummatory cues elicited by the biting and swallowing of prey. Specifically, we tested the
460 hypothesis that such ingestion cues might be necessary for the more sustained reciprocal
461 changes in LH and cH activities that accompany voracious feeding. Since consummatory
462 activity cannot be assessed in head-fixed animals, pERK analysis of activity was performed on
463 post-fixed animals after free-swimming hunting and feeding behaviors. To distinguish between
464 sensory and consummatory activities, we compared the neural activity of food-deprived fish
465 upon exposure to either paramecia or artemia. Artemia are live prey commonly used to feed
466 adult zebrafish, and are actively hunted by fish at all stages (Figure 4a, Video 2). They are
467 however too large to be swallowed and consumed by larvae. Thus, the comparison between
468 these two types of prey dissociates neural activity associated with prey detection and hunting
469 from the neural consequences of food ingestion.

470 We found that with exposure to artemia it was not possible to detect a change in cH
471 activity, but as observed above with live calcium imaging, exposure to this food cue in the
472 absence of ingestion induced a small increase in ILH neural activity and a larger increase in
473 mLH activity (Figure 4a-b). The artemia-induced hypothalamic activity was, however, less than
474 that observed with consumable prey (Fig 4a-b). These observations suggest that the mLH
475 responds primarily to sensory cues and/or induced hunting behavior whereas the induction of
476 ILH activity largely depends on consumption. These data are furthermore consistent with the
477 strong anti-correlation of cH with ILH activity (compared to mLH activity, Fig 3f), since both
478 respond more strongly to food consumption rather than sensory cues. Thus, in addition to
479 comprising distinct cell types (Figure 1- Figure Supplement 2), the ILH and mLH are also
480 selective for different food cues, raising the possibility that they could be further specialized for
481 distinct behavioral functions (Figure 4c, also see Discussion).



482

483

484

485

486

487

488

489

490

491

492

493

494

495

496

497

498

499

Figure 4: Sensory cues and food consumption differentially regulates cH and LH domains

(a) Representative images of pERK activity induced by parametia vs artemia larvae. Hatched artemia are sensed and actively hunted by 7-8 dpf larval zebrafish, but too large to consume, allowing for the dissociation of sensory cues/hunting behavior and food consumption. Scale bar = 50 μm . Rightmost panel: Larval zebrafish attempt to hunt live artemia, performing J-bends and pursuits with eyes converged (Bianco et al., 2011). Also see Video 2.

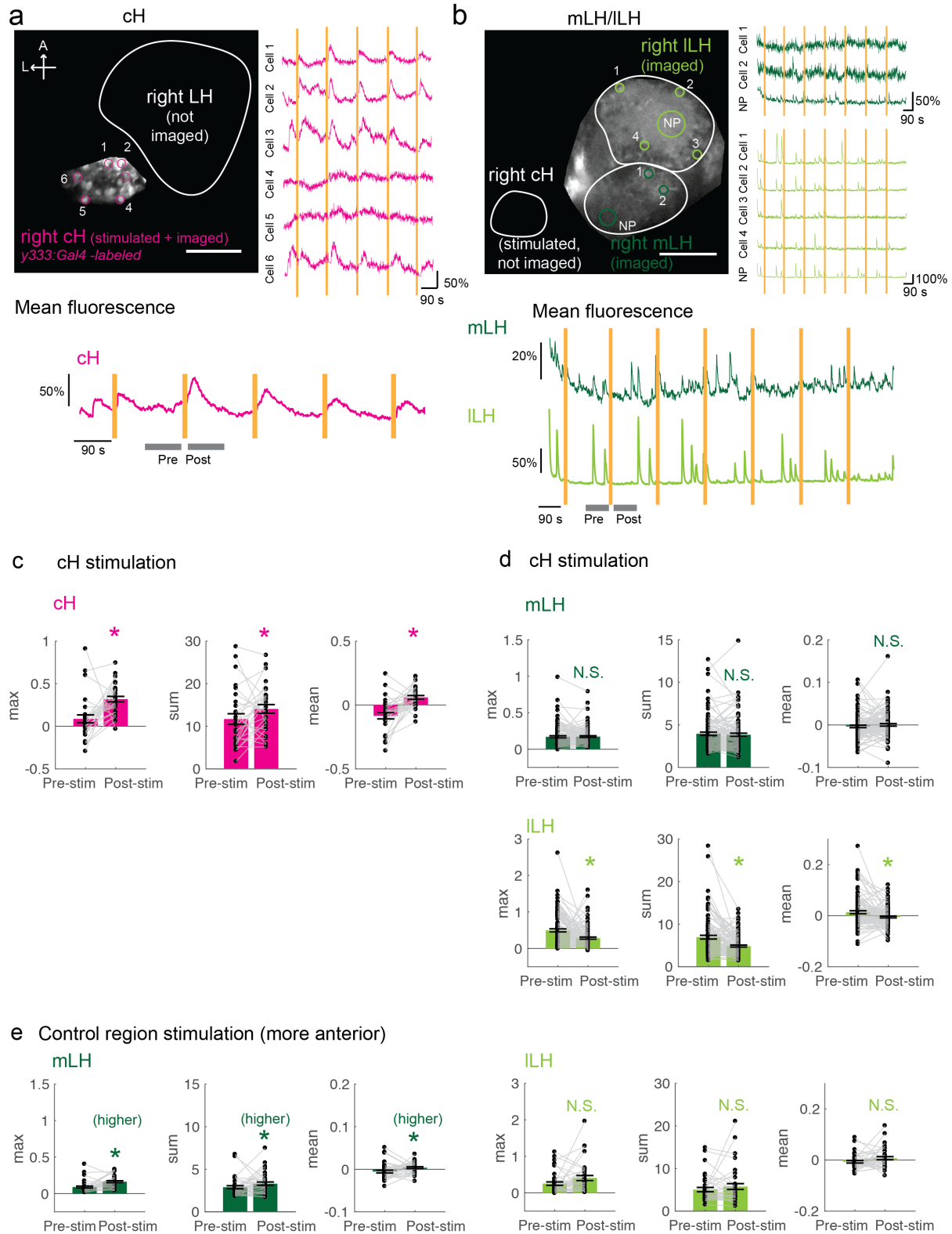
(b) cH activity (normalized pERK intensity) is significantly reduced by parametia but not by artemia ($p = 0.016$ (parametia), 0.648 (artemia)). In contrast, the LH can be activated by artemia alone, though more strongly in the presence of parametia. The ILH is more weakly activated than the mLH by artemia. Both normalized pERK intensity (mLH: $p = 2.06 \times 10^{-5}$ (parametia), $p = 4.87 \times 10^{-4}$ (artemia); ILH: $p = 2.06 \times 10^{-5}$ (parametia), $p = 0.033$ (artemia)), and active cell count (mLH: $p = 1.08 \times 10^{-5}$ (parametia), $p = 6.02 \times 10^{-5}$ (artemia); ILH: $p = 1.08 \times 10^{-5}$ (parametia), $p = 5.04 \times 10^{-5}$ (artemia)) are shown, with $n = 8/9/11$ fish, One-tail Wilcoxon Rank Sum Test).

(c) Revised schematic showing differential activation of cH and LH domains in response to food sensory vs consummatory cues.

500 ***Optogenetic cH activation suppresses ILH neural activity***

501 The anti-correlated activity of the caudal and lateral hypothalamus suggests they might
502 participate in mutual inhibition. We hypothesized that, during food deprivation, rising cH activity
503 (along with the absence of food cues) suppresses LH activity, whereas the arrival of food cues
504 and initial consumption that induces strong LH activity reciprocally shuts down cH activity. The
505 reduction in cH activity, in turn, would permit higher LH activity, which may underlie voracious
506 feeding behavior. Conversely, increased cH activity would reduce LH activity and return it to
507 satiety levels.

508 In order to test our model that activation of cH neurons is sufficient to suppress LH
509 activity, we expressed a red-shifted Channelrhodopsin (*Tg(UAS:ReaCHR-RFP)*) in cH neurons
510 (Dunn et al., 2016; Lin et al., 2013) and visualized LH neuronal activity via calcium imaging
511 using *Tg(HuC:GCaMP6s)*. Since expression of ReaChR by the *Tg(116A:Gal4)* driver line was
512 weak, we used a different Gal4 line, *Tg(y333:Gal4)*, that labels a smaller fraction of serotonergic
513 neurons in the cH ($57.4 \pm 2.1\%$), but drives robust ReaChR expression (Figure 5 – Figure
514 Supplement 1). In addition, the *Tg(UAS:GGaMP6s)* transgene was expressed in some animals,
515 allowing us to monitor optogenetically-induced cH activity. In these animals, ReaChR
516 stimulation (10-15 seconds, 633 nm laser illumination) and subsequent calcium imaging
517 confirmed strong activation of the cH. Significantly, optogenetic stimulation of the cH reduced
518 spontaneous ILH activity (Figure 5b, d), but did not alter mLH activity. Hence it appears that cH
519 activity is sufficient to inhibit ILH but not mLH activity. This distinction may allow mLH neurons to
520 remain sensitive and responsive to food cues under food-deprivation conditions, while cH
521 activity is elevated.



522
523
524
525
526

Figure 5 with 1 supplement: Optogenetic cH stimulation is sufficient to reduce ILH activity
(a) Stimulation of cH neurons in *Tg(y333:Gal4;UAS:ReaChR-RFP;UAS:GCaMP6s)* fish with a 633 nm laser induces sustained activation in a fraction of cells. Image shows confocal imaging and stimulation

527 area, numbers depict individual cells whose activities ($\Delta f/f$) are shown on the right. Scale bar = 50 μm .
528 Bottom: Mean fluorescence across the entire ROI over time. Orange bars = 10 second stimulation period
529 (no imaging occurs during that period). Gray bars indicate pre- and post-stimulation period over which
530 activity will be averaged.

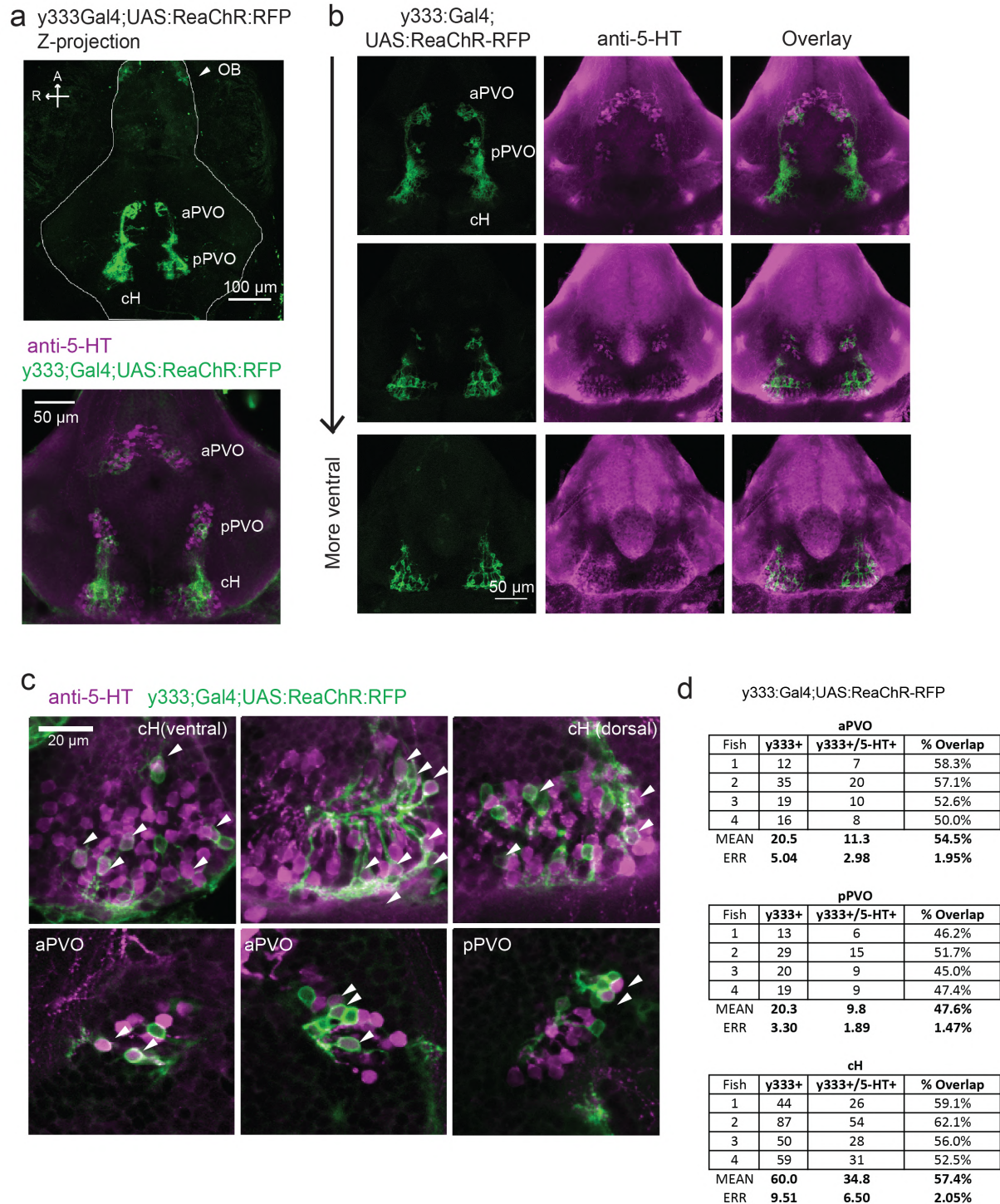
531 **(b)** Stimulation of cH neurons in a different fish expressing *Tg(y333:Gal4;UAS:ReaChR-RFP;*
532 *HuC:GCaMP6s)* reduces spontaneous activity in ILH neurons. The cH was not imaged simultaneously as
533 ReaChR can be activated by higher-intensity 488 nm light (see methods). Image shows confocal imaging
534 and stimulation area, numbers depict individual cells or neuropil (NP) whose activities ($\Delta f/f$) are shown on
535 the right. It was not always possible to resolve individual LH cells in other imaged fish. Scale bar = 50 μm .
536 Bottom: Mean fluorescence across mLH and ILH ROIs over time.

537 **(c-f)** Comparison of mean and maximum $\Delta f/f$ for a 90 s window before and after ReaChR stimulation.
538 Each data point represents a single stimulation.

539 **(c)** cH activity increases after ReaChR stimulation. $N = 29$ stimulations across 8 fish, $p =$
540 $0.0002(\text{max})/0.036(\text{sum})/9.2 \times 10^{-5}(\text{mean})$, One-tail Wilcoxon sign rank test.

541 **(d)** mLH activity does not change after ReaChR stimulation ($p = 0.74$ (max)/0.85 (sum)/0.13 (mean)),
542 whereas ILH activity is significantly suppressed after ReaChR stimulation ($p = 0.0003(\text{max})/1.8 \times 10^{-6}$
543 (sum)/0.049(mean)). $N = 108$ stimulations across 9 fish. Two-tail Wilcoxon sign rank test.

544 **(e)** Stimulation of a control area (i.e. more anterior to cH and unlabeled by ReaChR) tends to increase
545 activity in the mLH ($p = 0.0003(\text{max})/0.039(\text{sum})/0.039(\text{mean})$) and does not change ILH activity ($p =$
546 $0.099(\text{max})/0.65(\text{sum})/0.096(\text{mean})$). $N = 37$ stimulations from 5 fish. Two-tail Wilcoxon sign rank test.
547



548
549
550
551
552
553
554

Figure 5- Figure Supplement 1: Characterization of the *y333:Gal4* line

(a) We used an alternative cH-labeling Gal4 line, *Tg(y333:Gal4)* (Marquat et al (2015)), to drive *Tg(UAS:ReaChR-RFP)* expression, as we were unable to detect any ReaChR expression using *Tg(116A:Gal4)*. **Top**: Whole mount stack of a *Tg(y333:Gal4;UAS:ReaChR-RFP)* (green) shows relatively specific expression in the caudal hypothalamus, as well as some labeling in the olfactory bulb (white

555 arrow) and other scattered cells. Scale bar = 100 μm . Bottom: Z-projection image of a dissected fish
556 brain mounted ventral side up, with anti-5-HT staining shown in magenta. Scale bar = 50 μm .
557 **(b)** Overlap of *Tg(y333:Gal4;UAS:ReaChR-RFP)* (green) with anti-5-HT immunostaining (magenta) is
558 seen in all layers of the caudal hypothalamus, and also the paraventricular organ (PVO), though the
559 degree of overlap is less for the PVO. Each row shows a different Z-plane, moving from more dorsal to
560 more ventral. Dissected fish brains mounted ventral side up. Scale bar = 50 μm .
561 **(c)** Higher magnification image showing moderate overlap of *Tg(y333:Gal4;UAS:ReaChR-RFP)* with anti-
562 5-HT staining in the cH and PVO. Arrows indicate cells with overlapping RFP and 5-HT expression. Scale
563 bar = 20 μm .
564 **(d)** Quantification of overlap between 5-HT and *Tg(y333Gal4;UAS:ReaChR-RFP)* expression in the cH
565 and PVO.

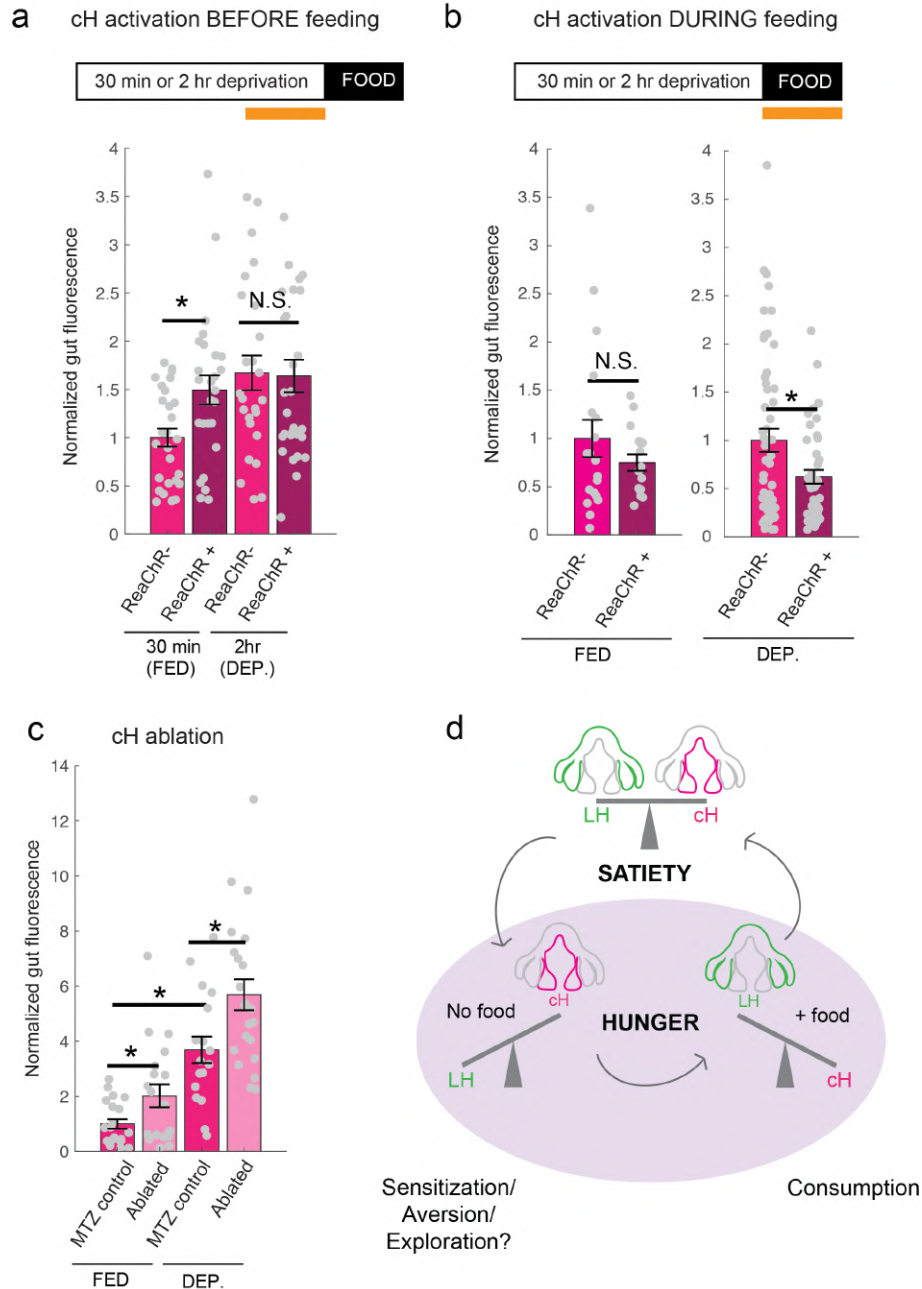
566 ***Functional dissection of cH serotonergic neurons in feeding behavior***

568 The opposing patterns of cH and LH activities suggest that they might have opposing roles in
569 the control of hunting and feeding behavior. Given that the cH is composed of neuromodulatory
570 populations, including serotonergic neurons, and is sufficient to suppress ILH neural activity, we
571 reasoned that these cH neurons might act as a homeostatic regulator of satiation state-
572 dependent food intake. In particular, we postulated that: 1) higher cH activation prior to feeding
573 would encode a state of hunger and enhance the animal's sensitivity to subsequent food cues,
574 and 2) higher cH activation during feeding would oppose ILH activity to suppress food intake. To
575 test this hypothesis, we combined ReaChR activation of cH neurons with quantitative
576 measurements of food intake, again using the *y333:Gal4* transgenic line. When satiated
577 (continuously fed) fish were exposed to whole field orange (630 nm) light for 10 minutes prior to
578 food presentation, fish in which ReaChR was expressed in the cH consumed significantly more
579 paramecia than fish that lacked *Tg(y333:Gal4;UAS:ReaChR-RFP)* expression (Figure 6a). This
580 effect was not observed for food-deprived fish, perhaps because they already display high cH
581 activity and a high rate of feeding (Figure 6a). These observations are consistent with the
582 interpretation that optogenetic cH activation simulated a food-deprived state in satiated fish and
583 thus enhanced their subsequent feeding.

584 In contrast to the outcome of optogenetic activation prior to feeding, the induction of cH
585 activity during food presentation reduced feeding, especially in food-deprived fish (Figure 6b).

586 These observations indicate that optogenetic cH activation can reduce feeding, particularly in
587 animals in which cH activity is low (Figure 6b, Figure 6 - Figure Supplement 1). Accordingly, we
588 propose that optogenetic stimulation of cH activity inhibits ILH activity and thereby causes the
589 feeding rate to decrease.

590 Finally, we asked what would happen if we directly reduced net cH activity via partial
591 ablation of the serotonergic population. We hypothesized that this would induce a constitutively
592 low cH activity, which should enhance food intake regardless of satiation state. Thus, we
593 performed chemical-genetic ablations of serotonergic cH neurons labeled by *Tg(116A:Gal4;*
594 *UAS:nfsb-Cherry)* (Curado et al., 2008), and compared the feeding rates of ablated animals to
595 that of sibling controls (Figure 6c). Food ingestion was examined in animals in which cH
596 neurons were partially ablated (see Figure 6 - Figure Supplement 2 and legend for details) and
597 compared to that of their non-ablated siblings, who lacked *Tg(116A:Gal4;UAS:nfsb-Cherry)*
598 expression (Figure 6c). We observed a significantly increased food intake for ablated fish in
599 both food-deprived and fed conditions, indicating that regardless of prior activity patterns, low
600 cH activity in the presence of food is what ultimately controls food consumption.



601

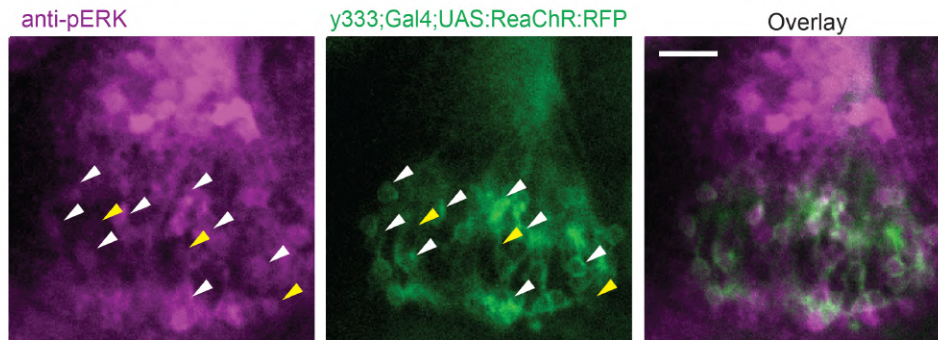
602 **Figure 6 with 3 supplements: Role of the cH in behavioral control**

603 **(a)** Optogenetic activation (orange bar in schematic) of the cH 10 min prior to feeding increases food
 604 intake in fed fish, but not food-deprived fish, during subsequent food presentation. Fed: n = 27/26
 605 (ReaChR-/ReaChR+), p = 0.005. Food-deprived: n = 25/29 (ReaChR-/ReaChR+), p = 0.36, One-tail
 606 Wilcoxon Rank Sum Test. Since ReaChR expression via 116A:Gal4 was negligible, we used another
 607 Gal4 (*Tg(y333:Gal4)*) line that is also specific to the cH when ReaChR is expressed. Fed and food-
 608 deprived fish were assayed simultaneously, thus all results was normalized to fed controls. ReaChR-
 609 controls do not have visible *Tg(y333:Gal4;UAS:ReaChR-RFP)* expression, and thus are a mixture of
 610 siblings expressing *Tg(y333:Gal4) only*, *Tg(UAS:ReaChR-RFP)* or neither of these transgenes, each with
 611 $\frac{1}{3}$ probability.

612 **(b)** Left: Optogenetic activation of the cH (orange bar in schematic) during feeding in fed fish does not

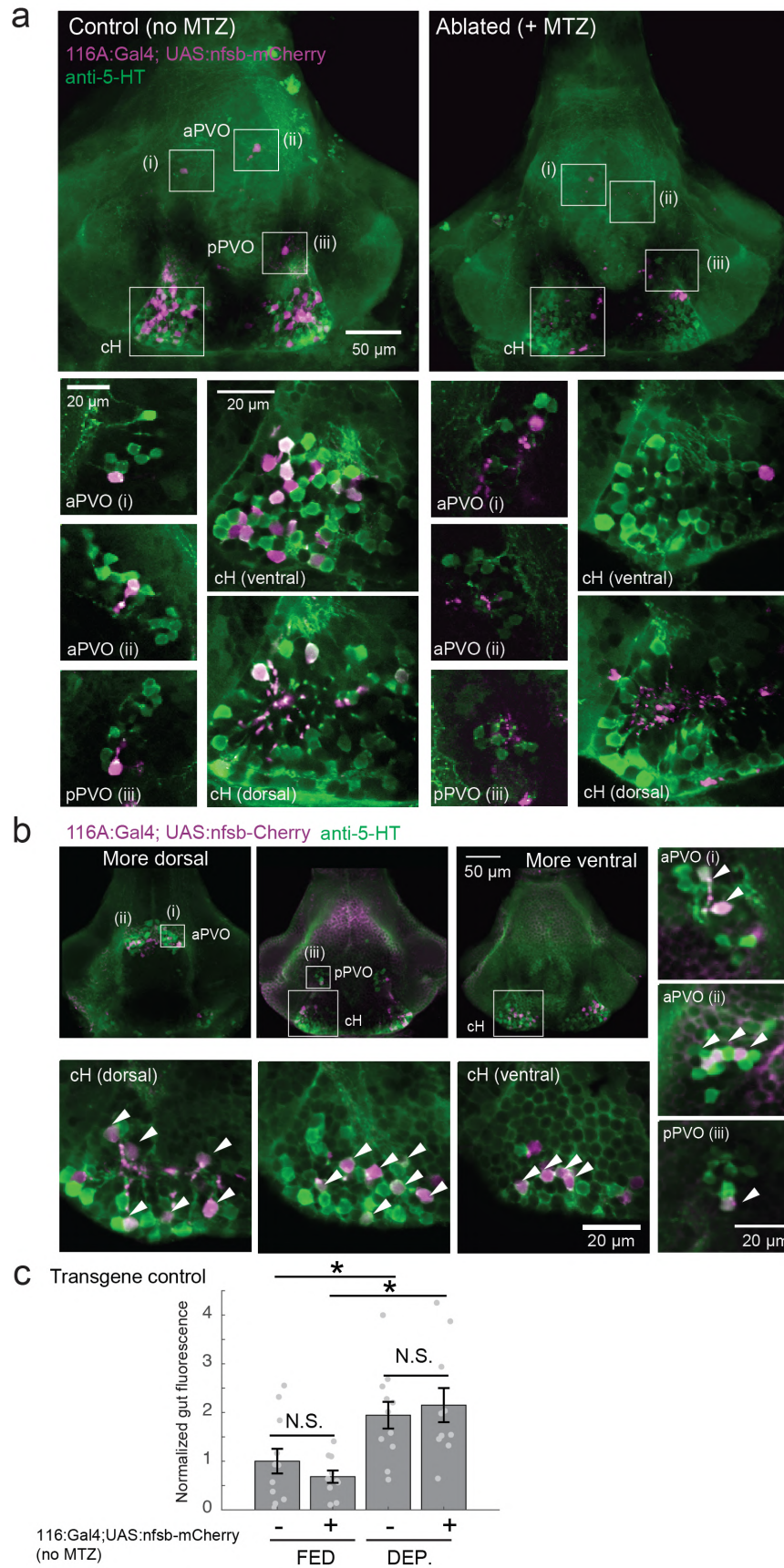
613 significantly reduce food intake. $n = 19/16$ (ReaChR-/ReaChR+), $p = 0.44$ (N.S.), Right: Optogenetic
614 activation of the cH during feeding in food-deprived fish reduces food intake. $n = 53/44$ (ReaChR-
615 /ReaChR+), $p = 0.042$. Since fed and food-deprived fish were assayed in different experiments, gut
616 fluorescence normalized to their respective controls, One-tail Wilcoxon Rank Sum Test.
617 **(c)** Nitroreductase-mediated ablation of the cH in (*Tg(116A:Gal4;UAS:nfsb:mCherry)* or negative fish
618 treated with metronidazole from 5-7 dpf significantly enhances food intake in 8 dpf fish. $p =$
619 $0.004/0.04/1.4 \times 10^{-5}$ (fed control vs ablated, dep. control vs ablated, fed vs dep.). Controls do not have
620 visible *Tg(116A:Gal4;UAS:nfsb-mcherry)* expression, and thus are a mixture of siblings expressing
621 *Tg(116A:Gal4)* only, *Tg(UAS:nfsb-mcherry)* or neither of these transgenes, each with $\frac{1}{8}$ probability.
622 **(d)** Schematic summarizing our results. We propose distinct roles of the cH during hunger, depending on
623 the presence or absence of food. See Supplementary Document 1 – Conceptual Circuit Model for
624 elaboration.
625

a Whole-field optogenetic illumination

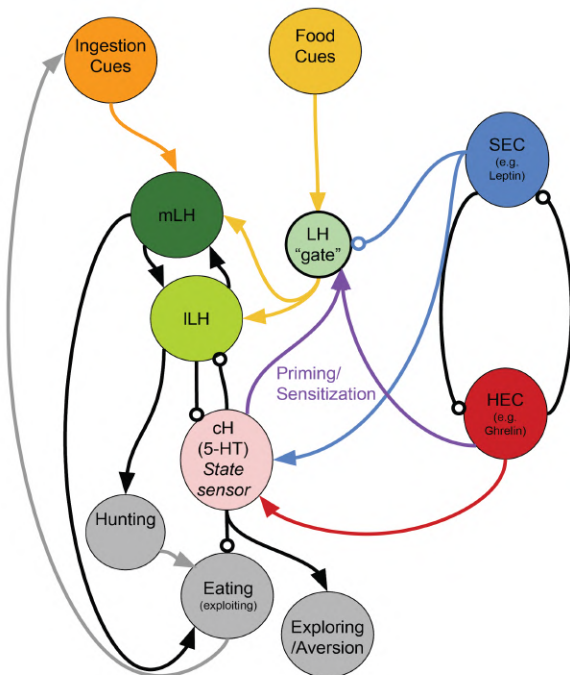


626
627

628 **Figure 6 – Figure Supplement 1: ReaChR activation by whole-field optogenetic illumination**
629 **(a)** *Tg(y333:Gal4;UAS:ReaChR-RFP)* stimulation during feeding is sufficient to induce pERK activity in
630 many transgene-positive neurons. White arrows point to a few examples where *Tg(y333:Gal4;ReaChR-*
631 *RFP)* expression corresponds to more intense pERK staining. Yellow arrows point to examples in which
632 ReaChR expression is visibly absent, which appears to correspond to weaker pERK staining. ReaChR
633 expression looks hazy as it was photobleached by the end of the 10 min stimulation period. Scale bar =
634 20 μm .
635



637 **Figure 6 - Figure Supplement 2: Nitroreductase-mediated ablation of cH neurons**
 638 **(a)** Effective ablation of *Tg(116A:Gal4;UAS:nfsb-mCherry)*-labeled neurons using MTZ. Note that due to
 639 sparser expression, ablation of the cH/PVO populations are likely to be partial (<50%). Representative
 640 projection images are shown of non-ablated (left) and ablated fish brains (right). Scale bar = 50 μ m.
 641 Insets roughly labeled by white boxes show higher-magnification single-plane images of cH, aPVO and
 642 pPVO labeling by this transgene, and overlap with 5-HT expression. Overall, since the labeling of cH
 643 neurons with nitroreductase-mCherry is relatively weak (~ 6-8 cells in the aPVO, ~2-4 cells in pPVO, and
 644 ~30-40 cells in the cH), our ablations are only partial and may include a few PVO neurons. Scale bar = 20
 645 μ m.
 646 **(b)** Similar to *Tg(116A:Gal4;UAS:GFP)*, there is high overlap of *Tg(116A:Gal4;UAS:nfsb-mCherry)* with
 647 anti-5-HT immunostaining. Scale bar = 50 μ m. Insets roughly labeled by white boxes show higher-
 648 magnification single-plane images of cH, aPVO and pPVO labeling by this transgene, and overlap with 5-
 649 HT expression. Scale bar = 20 μ m.
 650 **(c)** The *Tg(116A:Gal4;UAS:nfsb-mCherry)* transgene does not affect feeding in the absence of MTZ,
 651 relative to non-expressing siblings. Fed: $p = 0.64$, $n = 11$ (negative)/10(positive); Dep.: $p = 0.91$, $n =$
 652 11(negative)/10(positive), Fed vs Dep.: $p = 0.035$ (negative)/ 7.7×10^{-4} (positive).
 653



654 **Figure 6 - Figure Supplement 3: A conceptual circuit model of the cH/LH hypothalamic network**
 655 HEC = Hunger Encoding Circuit, SEC = Satiety Encoding Circuit, which should have anti-correlated
 656 activities and report the animal's energy/caloric status. The cH represents both hunger and satiety state
 657 and sensitizes (or primes) the LH during hunger. It may drive other behaviors such as exploration or
 658 aversive behavior, but also suppresses feeding. Other HEC components may also be involved in LH
 659 sensitization. We propose mutual inhibition between the cH and LH, though we have only demonstrated
 660 unidirectional inhibition (cH on ILH) thus far. The mLH, normally responsive to food cues, may promote
 661 hunting, though not necessarily coupled with ingestion, whereas the ILH, which is more responsive to
 662 ingestive cues, should enhance further ingestion (i.e. eating). The LH "gate" is a conceptual
 663 representation of how its sensitivity to food cues could be modulated by other signals (i.e. reduced by the
 664 SEC and enhanced by cH-mediated sensitization). It does not necessarily represent a physical neuronal
 665 population. More elaboration can be found in Supplementary Document 1 – Conceptual Circuit Model.
 666
 667

668 **DISCUSSION**

669 Decades-old studies on appetite regulation in mammals have suggested modular hypothalamic
670 units that work to suppress or enhance food intake respectively. Here, we show that the larval
671 zebrafish hypothalamic network can similarly be functionally divided into its medial and lateral
672 units. These units show anti-correlated activity patterns during various states that relate to
673 ingestive behavior, such as hunger and voracious eating, and energy homeostasis is reflected
674 by a restoration of balance between these areas (Figure 6d). Furthermore, we show that within
675 these broad neural response classes lies a diversity of neurons that encode specific stimuli and
676 perform distinct functions depending on the timing of activation.

677

678 *Mutually opposing hypothalamic networks control zebrafish appetite*

679 We show that the medial hypothalamic zone, especially the caudal hypothalamus (cH) in the
680 zebrafish, is strongly activated by food-deprivation, and strongly inhibited during voracious
681 feeding, and that this happens on a timescale of seconds to minutes. Here, we focused mainly
682 on the serotonergic cH neurons, although many medially localized neurons may show similar
683 activity patterns. In contrast, the lateral hypothalamus (LH), which contains GABAergic and
684 glutamatergic neurons, is inhibited in the absence of food and most strongly activated during
685 voracious eating. Interestingly, satiated fish exhibit intermediate activity levels in both
686 hypothalamic regions. Thus, hunger in the presence and absence of food is represented by two
687 distinct states of activity in opposing brain regions, with restoration of energy homeostasis
688 paralleled by a balance of the network.

689 While generally anti-correlated, the cH and LH also appear to be differentially modulated
690 by both internal (i.e. hunger cues) and external factors (i.e. food). In the absence of food, LH
691 cellular activity decreases rapidly, suggesting a requirement of food/other external cues to drive
692 LH activity, though some modest rate of spontaneous activity is still observed. On the other
693 hand, the slower timescales of cH activation appears to reflect the animal's rising caloric deficit.

694 Notably, many of the cH neurons are cerebrospinal fluid-contacting and thus have access to
695 circulatory information (Lillesaar, 2011; Pérez et al., 2013).

696 Further, despite clear reductions in pERK cellular activity, calcium imaging has revealed
697 more complex dynamics of the LH over food-deprivation. These changes could be induced by
698 the generally aversive and potentially unnatural internal state of a head-fixed preparation, or,
699 more intriguingly, could reflect an increased sensitivity of LH neurons over the course of hunger.
700 These hypotheses can potentially be distinguished in future work by performing calcium imaging
701 of hunting and feeding behavior in a free-swimming setting (Kim et al., 2017).

702 Once food becomes available (but when caloric deficit is still high), a state change
703 occurs, and LH activity is strongly enhanced whereas cH activity is strongly suppressed.
704 Importantly, the degree of cH suppression and LH activation are correlated with the extent of
705 prior food-deprivation, suggesting a role for these nuclei in regulating food intake based on
706 caloric needs. This striking anti-correlation between the cH and LH suggests a mutual inhibition,
707 and that an acute reduction in cH activity is what allows for the enhanced LH release.

708 We have partially confirmed the hypothesis of such mutual inhibition using optogenetic
709 stimulation of the cH and simultaneous calcium imaging of the LH. We show that activation of
710 the cH is sufficient to drive down ILH, but not mLH activity. Consistent with these results, the cH
711 appears to be more strongly anti-correlated with the ILH than the mLH.

712 However, the mechanisms by which cH might influence LH activity, and vice versa, are
713 still unknown. It is possible that the cH may act via inhibitory GABAergic neurons, and/or exert
714 their effects through direct secretion of monoamines into the ventricles or perineuronal space.
715 The effect of cH optogenetic activation on ILH activity appears to persist for minutes, allowing
716 for the possibility of direct neuromodulatory action. At the same time, there appears to be a fast
717 (seconds) anti-correlation between cH and LH calcium activity, suggesting faster inhibitory
718 connections. The LH, which was previously characterized in Muto et. al (2017), similarly does
719 not appear to send direct projections to the cH, but could potentially interact via intermediary

720 neurons in the medial/periventricular regions of the hypothalamus.

721

722 *Food cues differentially regulate cH and LH domains*

723 Ingestive behavior has been proposed to comprise a number of temporal stages: 1) the
724 initiation phase, triggered by energy deficit, in which the animal begins to forage; 2) the
725 procurement phases, triggered by the presence of food sensory cues, in which the animal seeks
726 and pursues food; and 3) the consummatory phase, which involves a more stereotyped motor
727 program (Berthoud, 2002; Watts, 2000). An animal's energy status is sensed internally and may
728 influence the initiation, procurement and consummatory stages of ingestive behavior. Thus, a
729 hungry animal will be more alert to food cues, seek food more persistently and also eat it more
730 voraciously.

731 In mammals, LH neurons are responsive to both external food sensory cues and
732 consummatory cues (Jennings et al., 2015). Here, we show that the LH lobes in zebrafish also
733 respond differentially to food cues in an anatomically segregated manner. In this “sensory”
734 stage, the mLH is already activated, which may reflect an enhanced sensitivity to food cues
735 during hunger. However, mLH activation during this sensory stage is not as strong as post-food
736 consumption. In contrast, the ILH is only weakly activated by food cues, and cH activity
737 transiently falls but remains overall high. Thus, taken together with our optogenetic and calcium
738 imaging data, the mutually inhibitory circuit model is most consistent between the cH and ILH
739 (though the mLH is still generally anti-correlation with cH activity, especially in the presence of
740 food).

741 Since ILH and cH activity are modulated within minutes of food consumption they are
742 unlikely to reflect satiety signals, and rather might play a role in further driving voracious food
743 consumption, at least until the activity of both populations returns to baseline. In contrast, the
744 mLH may play a role in enhancing the sensitivity of the animal to external food sensory cues,
745 even prior to initial food consumption.

746 It is unclear which consummatory cues modulate LH and cH activity. Based on live
747 imaging results from Muto et al (2017), the greatest enhancement of LH activity was observed
748 almost immediately (milliseconds to seconds) after paramecia consumption. Thus, the cue is
749 likely a fast pregastric signal (taste/tactile/swallowing), rather than postgastric absorption or
750 hormone secretion.

751

752 *Functional roles of the cH and LH in and beyond appetite control*

753 Finally, we test the hypothesis that the cH and LH form mutually antagonistic functional units
754 that dominate different phases of hunger and drive appropriate behavioral responses during
755 each phase. In particular, we show that the activation state of the cH is a crucial regulator of
756 satiation-state dependent food intake. Artificial cH activation in satiated fish *prior* to feeding is
757 sufficient to drive subsequent voracious feeding. Based on observed cH dynamics, we propose
758 that the degree on cH inhibition during voracious feeding is proportional to the degree of cH
759 activation prior to feeding. This could be mediated by the release of serotonin/other
760 neuromodulators over the course of food-deprivation, which may be capable of sensitizing the
761 LH even in the absence of food cues. An intriguing, though untested hypothesis is that the rise
762 in LH calcium fluorescence during food-deprivation, that tends to parallel that of cH activity, may
763 reflect such sensitization. In this way, zebrafish are able to retain a “memory” of their hunger
764 state, which is released once food is presented, and up-regulate their feeding behavior
765 accordingly. This motif might help ensure that the animal eventually returns to a stable
766 equilibrium, that is, satiety.

767 We furthermore show that the acute effect of cH activation *during* feeding is suppression
768 of food intake, whereas cH ablation enhances food intake, which is again consistent with
769 mammalian studies of medial hypothalamic areas. At first glance, the observation that the cH
770 acutely suppresses food intake is inconsistent with the idea that it is most active during hunger.
771 However, our optogenetic experiments show that the context of cH activation needs to be taken

772 into consideration, and can have opposing results on feeding. In the presence of food, activation
773 of the cH may simply drive down LH activity, hence reducing food intake. This is assuming that
774 any sensitizing effect of cH activation is weaker than the acute inhibitory effect of cH activation
775 on ILH activity, a conclusion that appears to be validated by our behavioral results.

776 The seemingly paradoxical roles of the cH during hunger may also make sense when
777 considering that, in the absence of food, consummatory behavior would in fact be
778 counterproductive. Thus, during food-deprivation, the cH may play complementary roles such as
779 the sensitization of the LH and/or other feeding-related circuits (as discussed above), or drive
780 alternative behavioral programs, like foraging or energy-conserving measures during this stage
781 of hunger (see Supplementary Document 1 - Conceptual Circuit Model for a more in-depth
782 discussion). Given that cH neurons appear also to be activated by aversive stimuli (Randlett et
783 al., 2015), it may also more generally encode a negative valence state in the absence of food.
784 Similar features of hunger-related (i.e. AgRP) neurons have also been described in mammals
785 (Betley et al., 2015; Chen et al., 2015; Dietrich et al., 2015; Mandelblat-Cerf et al., 2015).

786 Although the cH does not have an exact mammalian homolog, its functions have been
787 proposed to be adopted by other modulatory populations, such as the serotonergic raphe
788 nucleus in mammals (Gaspar and Lillesaar, 2012; Lillesaar, 2011). While known to be a potent
789 appetite suppressant, serotonin is also released during food deprivation, and has been shown to
790 enhance food-seeking behavior (Elipot et al., 2013; Katak et al., 1978; Pollock and Rowland,
791 1981; Voigt and Fink, 2015). Thus, our results showing opposing cH activity patterns during
792 hunger could reflect similarly complex roles of serotonin in zebrafish, potentially explaining
793 some of its paradoxical functions. The cH and PVO also express dopaminergic (intermingled
794 with 5-HT) and histaminergic neurons (in the surrounding cell-layer of the cH), which appear to
795 be densely interconnected (Kaslin and Panula, 2001). We note that our data, while confirming a
796 role of serotonergic neurons, does not rule out an involvement of these other neuromodulators
797 in appetite control.

798 Further, our results do not rule out the involvement of other circuits in appetite control; in
799 fact, they suggest that there are numerous players involved. For example, the PVO appears to
800 be modulated by food cues and food-deprivation, is anti-correlated with LH activity, and labeled
801 by our transgenic lines (albeit more sparsely), suggesting it may complement the role of the cH.
802 Our conclusions are also limited by available tools and methodologies -- since different
803 transgenic lines were utilized for stimulation and ablation, we cannot be certain that we are
804 manipulating the same population of neurons, though both share mutual overlap with
805 serotonergic cells. Also, due to the lack of complete transgene specificity, there is a possibility
806 that our manipulations may affect non-specific targets such as the olfactory bulb.

807 Similarly, while the strong LH activation after food-deprivation suggests that it might
808 promote voracious feeding, we were unable to assay the effect of LH activation in larval
809 zebrafish, due to broad and unspecific expression within the LH-labeling transgenic line.
810 However, Muto et al (2017) recently demonstrated that inhibition of the LH impairs prey capture
811 behavior, though they did not implicate the LH in the regulation of food intake based on hunger
812 state. Furthermore, electrical stimulation of the homologous region (lateral recess nuclei) in
813 adult cichlids and bluegills (Demski, 1973; Demski and Knigge, 1971) can elicit feeding
814 behavior, which is consistent with our hypothesis. Interestingly, while stimulating some of these
815 regions induced food intake, other induced behaviors, such as the “snapping of gravel”, were
816 reminiscent of food search or procurement. In mammals, electrical or optogenetic stimulation of
817 LH neurons triggers voracious eating, again consistent with our findings that the LH is highly
818 activated during the voracious eating phase in hungry fish (DELGADO and ANAND, 1953). In
819 particular, GABAergic neurons that do not co-express MCH or Orexin have been shown to be
820 responsive to food cues and are sufficient to stimulate food intake in mammals (Jennings et al.,
821 2015). Whether these GABAergic and glutamatergic neurons of the zebrafish LH co-express
822 other neuromodulators, as has been recently discovered in mammals (Mickelsen et al., 2019),
823 remains to be explored. Overall, these data suggest that the zebrafish LH may similarly play an

824 important role in driving food intake during hunger, despite some differences in peptidergic
825 expression from mammalian LH. Certainly, since cues such as water flow and optogenetic
826 stimulation light are sufficient to modulate cH and/or LH neurons, these hypothalamic loci are
827 likely also involved in other sensorimotor behaviors beyond appetite regulation.

828 In conclusion, we have shown here how anatomically segregated hypothalamic networks
829 might interact to control energy homeostasis. We argue that the medial-lateral logic of
830 hypothalamic function may be conserved even in non-mammalian vertebrates, though their
831 activity patterns may possibly be more complex than originally believed. Our data suggests
832 diverse roles of neuromodulators such as serotonin in regulating behavioral responses during
833 hunger, which may complement mammalian observations. Finally, we propose that investigating
834 large-scale network dynamics may reveal an additional layer of insights into the principles
835 underlying homeostatic behavior, which might be overlooked when studies are restricted to the
836 observation and perturbation of a small subpopulation.

837 838 **SUPPLEMENTARY FIGURE LEGENDS**

839
840 **Supplementary Table 1:** Z-brain anatomical regions that are more activated in voraciously
841 feeding (food-deprived + food) fish as compared to fed fish.

842
843 **Supplementary Table 2:** Z-brain anatomical regions that are more activated in fed fish as
844 compared to voraciously feeding (food-deprived + food) fish.

845
846 **Video 1:** Z-stack (dorsal to ventral) of brain activity map shown in Figure 1b.

847
848 **Video 2:** Video of larval zebrafish hunting artemia larvae. Prey-capture behavior, such as J-
849 bends and pursuits, but no capture swims, were observed in response to artemia larvae.
850 Recording rate: 30 fps. Playback rate: Real time.

851 852 **Supplementary File 1: Conceptual Circuit Model**

853 A comprehensive overview of our circuit model and current understanding, including a circuit
854 diagram, detailed elaboration and testable predictions.

855
856
857
858

859 **MATERIALS AND METHODS**

860

861 **Key Resource Table**

Reagent type (species) or resource	Designation	Source or reference	Identifiers	Additional information
genetic reagent (<i>danio rerio</i>)	<i>Tg(pGal4FF:116A)</i>	Characterized in this manuscript		Dr. Koichi Kawakami (NIG, Japan)
genetic reagent (<i>danio rerio</i>)	<i>Tg(pGal4FF:76A)</i>	PMID: 28425439		Dr. Koichi Kawakami (NIG, Japan)
genetic reagent (<i>danio rerio</i>)	<i>Tg(y333:Gal4)</i>	PMID: 26635538		Dr. Harold Burgess (NIH)
genetic reagent (<i>danio rerio</i>)	<i>Tg(HuC:GCaMP6s)</i>	PMID: 28892088		Dr. Florian Engert (Harvard)
genetic reagent (<i>danio rerio</i>)	<i>Tg(UAS:GCaMP6s)</i>	PMID: 28425439		Dr. Koichi Kawakami (NIG, Japan)
genetic reagent (<i>danio rerio</i>)	<i>Tg(UAS:GCaMPHS)</i>	PMID: 22046464		Dr. Koichi Kawakami (NIG, Japan)
genetic reagent (<i>danio rerio</i>)	<i>Tg(UAS:ReaChR-RFP)</i>	Characterized in this manuscript		Dr. Misha Ahrens (Janelia Research Campus)
genetic reagent (<i>danio rerio</i>)	<i>Tg(UAS-E1b:NTR-mCherry)</i>	PMID: 17335798		Available from ZIRC
genetic reagent (<i>danio rerio</i>)	<i>Tg(Vglut2a:dsRed)</i>	PMID: 19369545		
genetic reagent (<i>danio rerio</i>)	<i>Tg(Gad1b:loxP-dsRed-loxP-GFP)</i>	PMID: 23946442		
genetic reagent (<i>danio rerio</i>)	<i>Tg(Gad1b:GFP)</i>	PMID: 23946442		
genetic reagent (<i>danio rerio</i>)	<i>Tg(TH2:GCamP5)</i>	PMID: 26774784		Dr. Adam Douglass (University of Utah)

genetic reagent (<i>danio rerio</i>)	<i>Tg(ETvmat2:GFP)</i>	PMID:18164283		
genetic reagent (<i>danio rerio</i>)	<i>Tg(HCRT:RFP)</i>	PMID: 25725064		
antibody	Rabbit polyclonal anti-pERK	Cell Signaling	4370 RRID:AB_2315112	IHC(1:500)
antibody	mouse monoclonal anti-ERK	Cell Signaling	4696 RRID:AB_390780	IHC (1:500)
antibody	rabbit polyclonal anti-5-HT	Sigma-Aldrich	S5545 RRID:AB_477522	IHC (1:500)
antibody	goat polyclonal anti-5-HT	AbCam	ab66047 RRID:AB_1142794	IHC(1:500), 2% BSA in PBS blocking solution)
antibody	goat polyclonal anti-MSH	EMD Millipore	AB5087 RRID:AB_91683	IHC(1:500), 2% BSA in PBS blocking solution)
antibody	rabbit polyclonal anti-AGRP	Phoenix Pharmaceuticals	H-003-53 RRID:AB_2313908	IHC (1:500)
antibody	rabbit polyclonal anti-MCH	Phoenix Pharmaceuticals	H-070-47 RRID:AB_1001363 2	IHC (1:500)
antibody	rabbit polyclonal anti-CART	Phoenix Pharmaceuticals	55-102 RRID:AB_2313614	IHC (1:500)
antibody	rabbit polyclonal anti-NPY	Immunostar	22940 RRID:AB_2307354	IHC (1:500)
antibody	mouse monoclonal anti-TH	Immunostar	22941 RRID:AB_1624244	IHC (1:500)
chemical compound, drug	DiD' solid (lipid dye)	Thermo Fisher Scientific	D-7757	Stock solution (10mg/ml), working solution (2.5mg/ml), in ethanol

862

863 *Fish husbandry and transgenic lines*

864

865 Larvae and adults were raised in facility water and maintained on a 14:10 hr light:dark cycle at

866 28°C. All protocols and procedures involving zebrafish were approved by the Harvard
867 University/Faculty of Arts & Sciences Standing Committee on the Use of Animals in Research
868 and Teaching (IACUC). WIK wildtype larvae and *mit1fa*^{-/-} (*nacre*) larvae in the AB background,
869 raised at a density of ~40 fish per 10 cm petri dish, were used for behavioral and MAP-
870 mapping experiments.

871
872 Transgenic lines *Tg(UAS-E1b:NTR-mCherry)*(Davison et al., 2007) (referred to as UAS:nfsb-
873 mCherry), *Tg(UAS:GCaMPHS)* and *Tg(UAS:GCaMP6s)*(Muto and Kawakami, 2011; Muto et al.,
874 2017), *Tg(HuC:GCaMP6s)*(Kim et al., 2017), *Tg(Vglut2a:dsRed)* (Miyasaka et al., 2009),
875 *Tg(Gad1b:loxP-dsRed-loxP-GFP)* and *Tg(Gad1b:GFP)* (Satou et al., 2013), *Tg(TH2:GCamp5)*
876 (McPherson et al., 2016), *Tg(ETvmat2:GFP)* (referred to as VMAT:GFP) (Wen et al., 2008),
877 *Tg(HCRT:RFP)* (Liu et al., 2015) have all been previously described and characterized.
878 *Tg(pGal4FF:116A)* (referred to as 116A:Gal4) was isolated from a gene trap screen by the
879 Kawakami group (Kawakami et al., 2010); *Tg(pGal4FF:76A)* was recently published by the
880 same group(Muto et al., 2017). *Tg(y333:Gal4)* from a different enhancer trap screen was used
881 to drive expression in the cH in cases where 116A:Gal4-driven expression was sparse
882 (Marquart et al., 2015). *Tg(UAS:ReaChR-RFP)* was a gift from Misha Ahrens and Chao-Tsung
883 Yang, made using Tol2 transgenesis in the Ahrens lab at Janelia Research Campus. The same
884 construct was previously validated in Dunn et al, 2016.

885

886 MAP-mapping of appetite regions

887

888 More details on the MAP-mapping procedure can be found in Randlett et al (2015). 5-6 dpf,
889 *mit1fa*^{-/-} (*nacre*) larvae in the AB background larvae were fed an excess of paramecia once
890 daily. On the day of the experiment (at 7dpf), the larvae were distributed randomly into two
891 treatment groups: 1) FOOD-DEPRIVED, where larvae were transferred into a clean petri dish of
892 facility water, taking care to rinse out all remaining paramecia or 2) FED, where after washing
893 and transferring they were fed again with an excess of paramecia. After two hours, larvae in
894 both groups were fed with paramecia. After 15 minutes, larvae were quickly funneled through a
895 fine-mesh sieve, and the sieve was then immediately dropped into ice-cold 4%
896 paraformaldehyde (PFA) in PBS (PH 7.2-7.4). Fish were then immunostained with procedures
897 as reported below (see Immunostaining methods). The rabbit anti-pERK antibody (Cell
898 Signaling, #4370) and mouse anti-ERK (p44/42 MAPK (Erk1/2) (L34F12) (Cell Signaling,
899 #4696) were used at a 1:500 dilution. Secondary antibodies conjugated with alexa-fluorophores
900 (Life Technologies) were diluted 1:500. For imaging, fish were mounted dorsal-up in 2% (w/v)
901 low melting agarose in PBS (Invitrogen) and imaged at ~0.8/0.8/2 µm voxel size (x/y/z) using an
902 upright confocal microscope (Olympus FV1000), using a 20x 1.0NA water dipping objective. All
903 fish to be analyzed in a MAP-Mapping experiment were mounted together on a single imaging
904 dish, and imaged in a single run, alternating between treatment groups.

905

906 Whole-mount Immunostaining

907

908 24 hours after fixation (4% paraformaldehyde (PFA) in PBS), fish were washed in PBS + 0.25%
909 Triton (PBT), incubated in 150mM Tris-HCl at pH 9 for 15 min at 70°C (antigen retrieval),

910 washed in PBT, permeabilized in 0.05% Trypsin-EDTA for 45 min on ice, washed in PBT,
911 blocked in blocking solution (10% Goat Serum, 0.3% Triton in BSS or 2% BSA in PBS, 0.3%
912 Triton) for at least an hour and then incubated in primary and secondary antibodies for up to 3
913 days at 4°C diluted in blocking solution. In-between primary and secondary antibodies, fish were
914 washed in PBT and blocked for an hour. If necessary, pigmented embryos were bleached for 5
915 min after fixation with a 5%KOH/3%H₂O₂ solution.

916
917 The protocol was similar for dissected brains, except that the brains were dissected in PBS after
918 24 hours of fixation, and the Tris-HCL antigen retrieval/permeabilization step in Trypsin-EDTA
919 was omitted. Dissected brains were mounted ventral up on slides in 70% glycerol prior to
920 imaging. Confocal images of dissected brains were obtained using either a Zeiss LSM 700 or
921 Olympus FV1000.

922
923 Quantification of 5-HT overlap with transgenic lines

924
925 The same individual manually quantified overlap of all transgenic lines with whole-mount or
926 dissected 5-HT staining, to maintain standardization.

927
928 Quantification of food intake

929
930 Paramecia cultures (~1-2 500 ml bottles) were harvested, spun down gently (<3000 rpm) and
931 concentrated, and subsequently incubated with lipid dye (DiD' solid, D-7757, Thermo Fisher
932 Scientific, dissolved in ethanol) for > 2 hrs (5 µl of 2.5mg/ml working solution per 1 ml of
933 concentrated paramecia) on a rotator with mild agitation. They were then spun down gently
934 (<3000 rpm), rinsed and reconstituted in deionized water. An equal amount (100µl, ~500
935 paramecia) was pipetted into each 10 cm dish of larvae. This method was adapted from
936 Shimada et al., 2012. After the experiment, larvae were fixed and mounted on their sides on
937 glass slides or placed in wells of a 96 well plate. They were then imaged using the AxioZoom
938 V16 (Zeiss) and analyzed using custom Fiji software (Schindelin et al., 2012). In cases where
939 identity of larvae needed to be maintained, for example, to correlate food intake with brain
940 activity, larvae were imaged and subsequently stained individually in 96 well plates. This led to
941 more variable staining which precludes analysis of mean fluorescence.

942
943 Larvae were always distributed randomly into experimental groups.

944
945 Quantification of LH and cH activity in dissected brains

946
947 Brains within each dataset were usually registered onto a selected reference image from the
948 same dataset using the same CMTK registration software used in MAP-mapping. Further
949 analysis was then performed using custom Fiji and MATLAB software.

950
951 For quantification of cH, mLH and pERK fluorescence intensity, ROIs were manually defined
952 using the reference image, and pERK intensity was quantified over all registered images and
953 averaged across the entire lobe (multiple z-planes) as well as across both lobes. Analysis of cH

954 pERK fluorescence was restricted to the most ventral planes, as more dorsal cH neurons show
955 weaker correlation with feeding states (as seen in Figure 2 – Figure Supplement 4).

956
957 For quantification of mLH and ILH active cell count, automated analysis of cell count was again
958 performed using custom Fiji software, namely: 1) Image processing to reduce background and
959 enhance contrast 2) Adaptive thresholding to isolate strongly-stained cells 3) Applying the
960 “Analyze Particles” function to quantify the number of cells within each manually-defined ROI.

961
962 Aggregation and visualization of results was performed using custom MATLAB software.

963
964 Note that, in experiments in which the data was collected without the tERK channel (e.g. from
965 Figure 2), thus prohibiting image registration, ROIs were drawn manually over each region
966 across all z-planes and averaged to obtain mean fluorescence values.

967 For Figure 2 - Figure Supplement 1, where individual fish were stained, all measurements,
968 including cell count, were made manually. In addition, background fluorescence was measured
969 for each sample and subtracted from measured values.

970
971 Calcium imaging

972
973 For confocal calcium imaging of the cH and LH simultaneously in the presence of food,
974 *Tg(76A:Gal4;116A:Gal4; UAS:GCaMP6s)* triple transgenic fish were embedded in 1.8%
975 agarose, with their eyes/nostrils were released. GCaMP activity from a single z-plane (where
976 the cH and LH neurons could be seen) was imaged using a confocal microscope (Olympus
977 FV1000) at 1 fps. After a 5 min habituation period and a 10 min baseline period, a dense drop of
978 paramecia was pipetted into the dish. Due to paramecia phototaxis, most of the paramecia
979 moved into close vicinity of the fish’s head under the laser, allowing for strong visual/olfactory
980 exposure to paramecia. After image registration (TurboReg Fiji Plugin, Thevenaz et al., 1998),
981 and downsampling (Fiji/MATLAB), manually-segmented ROIs were selected and total
982 fluorescence within the ROI was calculated. Cross-correlation and other analyses were
983 performed using custom MATLAB software.

984
985 For confocal calcium imaging of the caudal hypothalamus (Figure 2- Figure Supplement 3), 4 to
986 6 food-deprived (2-6 hrs) or fed larvae expressing *Tg(116A:Gal4; UAS:GCaMPHS)*, were
987 embedded in 1.5% agarose on a large petri dish, and a z-stack covering the entire caudal
988 hypothalamus imaged using multi-area time lapse imaging every 5 minutes for 2 hrs. Maximum
989 projection images from the timelapse series were aligned to the first image of the series and
990 total fluorescence of both caudal hypothalamic nuclei was subsequently measured using
991 manually-drawn ROIs in ImageJ, to obtain the average calcium activity for each fish at each
992 time point.

993
994 For 2P imaging of the cH and LH simultaneously in the absence of food (Figure 2 - Figure
995 Supplement 4-5), *Tg(76A:Gal4;116A:Gal4; UAS:GCaMP6s)* triple transgenic fish were
996 embedded in 1.8% agarose. GCaMP activity from either multiple slices (3 z-planes spanning a
997 ~20 μ m volume of the intermediate hypothalamus using an electrically-tunable liquid lens

998 (Edmund Optics, 83-922), 237 ms per z-plane) or a single z-plane where the cH and LH
999 neurons (1.5 fps) could be seen was imaged using custom 2P microscopes. After image
1000 registration and downsampling to cell-sized voxels (Fiji/MATLAB), manually segmented ROIs
1001 were selected and total fluorescence within the ROI was calculated. Clustering, spike detection
1002 and other analyses were again performed using custom MATLAB software.

1003

1004 Optogenetic stimulation and simultaneous calcium imaging

1005

1006 Optogenetic stimulation and calcium imaging was performed on a confocal microscope (Zeiss
1007 LSM 880) using a 633 nm laser for ReaChR activation, and a 488 nm laser for calcium imaging.
1008 *Tg(y333:Gal4;UASReaChR-RFP; HuCGCaMP6s)* triple-transgenic fish were used to record LH
1009 activity after ReaChR activation. As *Tg(HuC:GCaMP6)* does not label the cH, in some cases we
1010 used fish that also had *Tg(UAS:GCaMP6s)* co-expressed in cH, allowing for monitoring of cH
1011 activity directly.

1012

1013 The ReaChR activation spectrum is wide and 488 nm laser power at sufficiently high intensities
1014 is sufficient to activate ReaChR. Since *Tg(y333:Gal4;UASGCaMP6s)* is expressed strongly in
1015 the cH, weak 488 nm laser power can be used to monitor cH activity after ReaChR activation of
1016 cH. On the other hand, *Tg(HuC:GCaMP6s)* expression in the LH is considerably weaker than
1017 *Tg(UAS:GCaMP6s)* expression driven by *Tg(y333:Gal4)*, and recording LH activity requires high
1018 laser power. Thus, during LH recording trials, we could not simultaneously image the cH.

1019

1020 Fed fish were embedded in 1.8%-2% agarose, with tails, mouth and eyes freed, 15-20 minutes
1021 before imaging in the absence of food. For baseline recording, spontaneous activities in cH or
1022 LH were recorded. ReachR activation was then induced in one side of cH periodically for 10-15
1023 s, and ensuing activity in one or both sides of LH or cH was recorded continuously during
1024 intervals (of 120-180s) between stimuli.

1025

1026 Nitroreductase-mediated ablations

1027

1028 Larvae expressing *Tg(116A:Gal4;UAS:nfsb-mCherry)*, or their non-transgenic siblings were
1029 incubated in 2.5mM Metronidazole (Sigma-Aldrich, M3761) from 4-6 dpf/5-7 dpf. MTZ was
1030 subsequently washed out, and food intake was measured at 7 or 8 dpf. For these experiments,
1031 the MTZ-treated siblings were used as the control group. Each control or ablated group was
1032 food-deprived or fed for 2 hrs, and labeled food was added to quantify food intake. In the case
1033 of fed fish, unlabeled food was very gently washed out 15 mins before the experiment and the
1034 food-deprived fish were also agitated slightly to simulate a short washout.

1035

1036 Optogenetic stimulation with behavior

1037

1038 Optogenetic stimulation was done by placing a square LED panel (630 nm, 0.12mW/mm² driven
1039 at full current, Soda Vision, Singapore) directly on top of petri dishes containing ReaChR
1040 positive or negative fish, for 10 minutes continuously before or during feeding. We had
1041 attempted other methods of stimulating the fish (e.g. pulsed LED stimulation) but found that it

1042 was disruptive to behavior.

1043

1044 Artemia Hunting Video

1045

1046 7 dpf larval fish were food-deprived for 2 hours, acclimatized in 24 well plates for 30 minutes,
1047 and then fed either an excess of hatched artemia or paramecia. Raw videos of hunting behavior
1048 were then recorded for 10 min at 30 fps using a high-resolution monochrome camera (Basler
1049 acA4924) and custom Python-based acquisition software.

1050

1051 High-resolution behavioral tracking

1052

1053 We developed a system (Johnson et al., manuscript in preparation) in which a high-speed
1054 infrared camera moves on motorized rails to automatically track a zebrafish larvae in a large
1055 pool (300 x 300 x 4mm). A single fish is recruited to the arena center with motion cues delivered
1056 from a projector to initiate each trial. Paramecia are dispersed throughout the middle of the pool
1057 For analysis 60 Hz image frames are centered and aligned. In every frame, the tail was
1058 skeletonized and the gaze angle of each eye is calculated. The eyes can each move from
1059 around zero degrees (parallel to body-axis) to 40 degrees (converged for hunting). Each bout
1060 was then represented as a point in 220-dimensional posture space by accumulating 22 posture
1061 measurements (20 tail tangent angles to encode tail shape, and 2 eye gaze angles) across 10
1062 image frames (~167 ms) from the beginning of each bout. All bouts were then mapped to a 2-D
1063 space with t-distributed stochastic neighbor embedding (t-SNE). Four major hunting bout types
1064 can be identified from this embedding. Hunts begin with the “j-turn”, and fish follow and advance
1065 toward prey objects with “pursuit” bouts. Hunts end with an “abort” or a “strike”. When the fish is
1066 not actively involved in a hunt, it explores the arena with “exploratory” bouts. Fractions of
1067 hunting bouts were then compared between fed and food-deprived fish in 3-minute time bins
1068 over 45 min.

1069

1070 Statistics

1071

1072 All error bars show mean \pm SEM over fish. Significance was reported as follows: * $p < 0.05$.
1073 Significance was determined using the non-parametric Wilcoxon Sign Rank test for paired data
1074 and the Wilcoxon rank Sum test for independent samples. One-tail tests were performed in
1075 cases where there was a prior prediction regarding the direction of change. A one-or two-way
1076 ANOVA (Tukey-Kramer correction, MATLAB statistical toolbox) was used in cases where
1077 multiple comparisons were involved.

1078

1079 **ACKNOWLEDGEMENTS**

1080

1081 We thank Harold Burgess kindly provided us with the y333:Gal4 transgenic line. We further
1082 thank Thomas Panier who assisted Robert Johnson in construction of the rig used for high
1083 resolution behavioral imaging. Support from Steve Turney and the CBS imaging facility, and the
1084 Harvard Center for Biological Imaging were essential for the successful completion of many
1085 experiments. Finally, we would like to thank Jessica Miller, Steve Zimmerman, Karen Hurley

1086 and Brittany Hughes at Harvard for providing invaluable fish care.

1087

1088 **COMPETING INTERESTS**

1089 The authors declare no competing interests.

1090

1091

1092 **REFERENCES**

1093

1094 Ahima, R.S., and Antwi, D.A. (2008). Brain regulation of appetite and satiety. *Endocrinol. Metab.*

1095 *Clin. North Am.* 37, 811–823.

1096 Ammar, A.A., Södersten, P., and Johnson, A.E. (2001). Locus coeruleus noradrenergic lesions

1097 attenuate intraoral intake. *Neuroreport* 12, 3095–3099.

1098 ANAND, B.K., and BROBECK, J.R. (1951). Hypothalamic control of food intake in rats and cats.

1099 *Yale J. Biol. Med.* 24, 123–140.

1100 Berthoud, H.-R. (2002). Multiple neural systems controlling food intake and body weight.

1101 *Neurosci. Biobehav. Rev.* 26, 393–428.

1102 Betley, J.N., Xu, S., Cao, Z.F.H., Gong, R., Magnus, C.J., Yu, Y., and Sternson, S.M. (2015).

1103 Neurons for hunger and thirst transmit a negative-valence teaching signal. *Nature* 521, 180–

1104 185.

1105 Bianco, I.H., and Engert, F. (2015). Visuomotor Transformations Underlying Hunting Behavior in

1106 Zebrafish. *Curr. Biol.* 25, 831–846.

1107 Bianco, I.H., Kampff, A.R., and Engert, F. (2011). Prey capture behavior evoked by simple

1108 visual stimuli in larval zebrafish. *Front. Syst. Neurosci.* 5, 101.

1109 BROBECK, J.R., LARSSON, S., and REYES, E. (1956). A study of the electrical activity of the

1110 hypothalamic feeding mechanism. *J. Physiol.* 132, 358–364.

1111 Chen, Y., Lin, Y.-C., Kuo, T.-W., and Knight, Z.A. (2015). Sensory Detection of Food Rapidly

1112 Modulates Arcuate Feeding Circuits. *Cell* 160, 829–841.

1113 Davison, J.M., Akitake, C.M., Goll, M.G., Rhee, J.M., Gosse, N., Baier, H., Halpern, M.E.,

1114 Leach, S.D., and Parsons, M.J. (2007). Transactivation from Gal4-VP16 transgenic insertions

1115 for tissue-specific cell labeling and ablation in zebrafish. *Dev. Biol.* 304, 811–824.

1116 DELGADO, J.M.R., and ANAND, B.K. (1953). Increase of food intake induced by electrical

1117 stimulation of the lateral hypothalamus. *Am. J. Physiol.* 172, 162–168.

1118 Demski, L.S. (1973). Feeding and aggressive behavior evoked by hypothalamic stimulation in a

1119 cichlid fish. *Comp. Biochem. Physiol. Part A Physiol.* 44, 685–692.

1120 Demski, L.S., and Knigge, K.M. (1971). The telencephalon and hypothalamus of the bluegill

1121 (*Lepomis macrochirus*): evoked feeding, aggressive and reproductive behavior with

1122 representative frontal sections. *J. Comp. Neurol.* 143, 1–16.

1123 Dietrich, M.O., Zimmer, M.R., Bober, J., and Horvath, T.L. (2015). Hypothalamic Agrp neurons

1124 drive stereotypic behaviors beyond feeding. *Cell* 160, 1222–1232.

1125 Dockray, G.J. (2009). The versatility of the vagus. *Physiol. Behav.* 97, 531–536.

1126 Dunn, T.W., Mu, Y., Narayan, S., Randlett, O., Naumann, E.A., Yang, C.-T., Schier, A.F.,

1127 Freeman, J., Engert, F., and Ahrens, M.B. (2016). Brain-wide mapping of neural activity

1128 controlling zebrafish exploratory locomotion. *Elife* 5.

1129 Elipot, Y., Hinaux, H., Callebert, J., and Rétaux, S. (2013). Evolutionary shift from fighting to

1130 foraging in blind cavefish through changes in the serotonin network. *Curr. Biol.* 23, 1–10.

1131 Filosa, A., Barker, A.J., Dal Maschio, M., and Baier, H. (2016). Feeding State Modulates

1132 Behavioral Choice and Processing of Prey Stimuli in the Zebrafish Tectum. *Neuron* 90, 596–

1133 608.

1134 Gaspar, P., and Lillesaar, C. (2012). Probing the diversity of serotonin neurons. *Philos. Trans.*

1135 *R. Soc. Lond. B. Biol. Sci.* 367, 2382–2394.

- 1136 Hoebel, B.G. (1965). Hypothalamic Lesions by Electrocauterization: Disinhibition of Feeding and
1137 Self-Stimulation. *Science* *149*, 452–453.
- 1138 Jennings, J.H., Ung, R.L., Resendez, S.L., Stamatakis, A.M., Taylor, J.G., Huang, J., Veleta, K.,
1139 Kantak, P.A., Aita, M., Shilling-Scriver, K., et al. (2015). Visualizing Hypothalamic Network
1140 Dynamics for Appetitive and Consummatory Behaviors. *Cell* *160*, 516–527.
- 1141 Johnson, R., Linderman, S., Panier, T., Wee, C.L., Song, E.Y., Herrera, K., Miller, A., and
1142 Engert, F. Point Process Models of Larval Zebrafish Behavior: Structure on Many Scales.
1143 (Manuscript in Preparation)
- 1144 Jordi, J., Guggiana-Nilo, D., Soucy, E., Song, E.Y., Wee, C.L., and Engert, F. (2015). A high-
1145 throughput assay for quantifying appetite and digestive dynamics. *Am. J. Physiol. Regul. Integr.*
1146 *Comp. Physiol.* *ajpregu.00225.2015*.
- 1147 Jordi, J., Guggiana-Nilo, D., Bolton, A.D., Prabha, S., Ballotti, K., Herrera, K., Rennekamp, A.J.,
1148 Peterson, R.T., Lutz, T.A., and Engert, F. (2018). High-throughput screening for selective
1149 appetite modulators: A multibehavioral and translational drug discovery strategy. *Sci. Adv.* *4*,
1150 eaav1966.
- 1151 Kantak, K.M., Wayner, M.J., and Stein, J.M. (1978). Effects of various periods of food
1152 deprivation on serotonin turnover in the lateral hypothalamus. *Pharmacol. Biochem. Behav.* *9*,
1153 529–534.
- 1154 Kaslin, J., and Panula, P. (2001). Comparative anatomy of the histaminergic and other
1155 aminergic systems in zebrafish (*Danio rerio*). *J. Comp. Neurol.* *440*, 342–377.
- 1156 Kawakami, K., Abe, G., Asada, T., Asakawa, K., Fukuda, R., Ito, A., Lal, P., Mouri, N., Muto, A.,
1157 Suster, M.L., et al. (2010). zTrap: zebrafish gene trap and enhancer trap database. *BMC Dev.*
1158 *Biol.* *10*, 105.
- 1159 Kim, D.H., Kim, J., Marques, J.C., Grama, A., Hildebrand, D.G.C., Gu, W., Li, J.M., and Robson,
1160 D.N. (2017). Pan-neuronal calcium imaging with cellular resolution in freely swimming zebrafish.
1161 *Nat. Methods*.
- 1162 Krasne, F.B. (1962). General Disruption Resulting from Electrical Stimulus of Ventromedial
1163 Hypothalamus. *Science* *138*, 822–823.
- 1164 Lillesaar, C. (2011). The serotonergic system in fish. *J. Chem. Neuroanat.* *41*, 294–308.
- 1165 Lin, J.Y., Knutsen, P.M., Muller, A., Kleinfeld, D., and Tsien, R.Y. (2013). ReaChR: a red-shifted
1166 variant of channelrhodopsin enables deep transcranial optogenetic excitation. *Nat. Neurosci.* *16*,
1167 1499–1508.
- 1168 Liu, J., Merkle, F.T., Gandhi, A. V., Gagnon, J.A., Woods, I.G., Chiu, C.N., Shimogori, T., Schier,
1169 A.F., and Prober, D.A. (2015). Evolutionarily conserved regulation of hypocretin neuron
1170 specification by *Lhx9*. *Development* *142*, 1113–1124.
- 1171 Mandelblat-Cerf, Y., Ramesh, R.N., Burgess, C.R., Patella, P., Yang, Z., Lowell, B.B., and
1172 Andermann, M.L. (2015). Arcuate hypothalamic AgRP and putative POMC neurons show
1173 opposite changes in spiking across multiple timescales. *Elife* *4*, e07122.
- 1174 Marquart, G.D., Tabor, K.M., Brown, M., Strykowski, J.L., Varshney, G.K., LaFave, M.C.,
1175 Mueller, T., Burgess, S.M., Higashijima, S., and Burgess, H.A. (2015). A 3D Searchable
1176 Database of Transgenic Zebrafish Gal4 and Cre Lines for Functional Neuroanatomy Studies.
1177 *Front. Neural Circuits* *9*, 78.
- 1178 McPherson, A.D., Barrios, J.P., Luks-Morgan, S.J., Manfredi, J.P., Bonkowsky, J.L., Douglass,
1179 A.D., and Dorsky, R.I. (2016). Motor Behavior Mediated by Continuously Generated
1180 Dopaminergic Neurons in the Zebrafish Hypothalamus Recovers after Cell Ablation. *Curr. Biol.*
1181 *26*, 263–269.
- 1182 Mickelsen, L.E., Bolisetty, M., Chimileski, B.R., Fujita, A., Beltrami, E.J., Costanzo, J.T.,
1183 Naparstek, J.R., Robson, P., and Jackson, A.C. (2019). Single-cell transcriptomic analysis of
1184 the lateral hypothalamic area reveals molecularly distinct populations of inhibitory and excitatory
1185 neurons. *Nat. Neurosci.* *22*, 642–656.
- 1186 Miyasaka, N., Morimoto, K., Tsubokawa, T., Higashijima, S., Okamoto, H., and Yoshihara, Y.

1187 (2009). From the olfactory bulb to higher brain centers: genetic visualization of secondary
1188 olfactory pathways in zebrafish. *J. Neurosci.* 29, 4756–4767.
1189 Muto, A., and Kawakami, K. (2011). Imaging functional neural circuits in zebrafish with a new
1190 GCaMP and the Gal4FF-UAS system. *Commun. Integr. Biol.* 4, 566–568.
1191 Muto, A., Lal, P., Ailani, D., Abe, G., Itoh, M., and Kawakami, K. (2017). Activation of the
1192 hypothalamic feeding centre upon visual prey detection. *Nat. Commun.* 8, 15029.
1193 Pérez, M.R., Pellegrini, E., Cano-Nicolau, J., Gueguen, M.-M., Menouer-Le Guillou, D., Merot,
1194 Y., Vaillant, C., Somoza, G.M., and Kah, O. (2013). Relationships between radial glial
1195 progenitors and 5-HT neurons in the paraventricular organ of adult zebrafish - potential effects
1196 of serotonin on adult neurogenesis. *Eur. J. Neurosci.* 38, 3292–3301.
1197 Pollock, J.D., and Rowland, N. (1981). Peripherally administered serotonin decreases food
1198 intake in rats. *Pharmacol. Biochem. Behav.* 15, 179–183.
1199 Randlett, O., Wee, C.L., Naumann, E.A., Nnaemeka, O., Schoppik, D., Fitzgerald, J.E.,
1200 Portugues, R., Lacoste, A.M.B., Riegler, C., Engert, F., et al. (2015). Whole-brain activity
1201 mapping onto a zebrafish brain atlas. *Nat. Methods* 12, 1039–1046.
1202 Satou, C., Kimura, Y., Hirata, H., Suster, M.L., Kawakami, K., and Higashijima, S. (2013).
1203 Transgenic tools to characterize neuronal properties of discrete populations of zebrafish
1204 neurons. *Development* 140, 3927–3931.
1205 Schindelin, J., Arganda-Carreras, I., Frise, E., Kaynig, V., Longair, M., Pietzsch, T., Preibisch,
1206 S., Rueden, C., Saalfeld, S., Schmid, B., et al. (2012). Fiji: an open-source platform for
1207 biological-image analysis. *Nat. Methods* 9, 676–682.
1208 Semmelhack, J.L., Donovan, J.C., Thiele, T.R., Kuehn, E., Laurell, E., and Baier, H. (2015). A
1209 dedicated visual pathway for prey detection in larval zebrafish. *Elife* 4.
1210 Shimada, Y., Hirano, M., Nishimura, Y., and Tanaka, T. (2012). A high-throughput fluorescence-
1211 based assay system for appetite-regulating gene and drug screening. *PLoS One* 7, e52549.
1212 Sternson, S.M., and Eiselt, A.-K. (2017). Three Pillars for the Neural Control of Appetite. *Annu.*
1213 *Rev. Physiol.* 79, 401–423.
1214 Stuber, G.D., and Wise, R.A. (2016). Lateral hypothalamic circuits for feeding and reward. *Nat.*
1215 *Neurosci.* 19, 198–205.
1216 TEITELBAUM, P., and EPSTEIN, A.N. (1962). The lateral hypothalamic syndrome: recovery of
1217 feeding and drinking after lateral hypothalamic lesions. *Psychol. Rev.* 69, 74–90.
1218 Thevenaz, P., Ruttimann, U.E., and Unser, M. (1998). A pyramid approach to subpixel
1219 registration based on intensity. *IEEE Trans. Image Process.* 7, 27–41.
1220 Trivedi, C.A., and Bollmann, J.H. (2013). Visually driven chaining of elementary swim patterns
1221 into a goal-directed motor sequence: a virtual reality study of zebrafish prey capture. *Front.*
1222 *Neural Circuits* 7, 86.
1223 Voigt, J.-P., and Fink, H. (2015). Serotonin controlling feeding and satiety. *Behav. Brain Res.*
1224 277, 14–31.
1225 Watts, A.G. (2000). Understanding the neural control of ingestive behaviors: helping to separate
1226 cause from effect with dehydration-associated anorexia. *Horm. Behav.* 37, 261–283.
1227 Wen, L., Wei, W., Gu, W., Huang, P., Ren, X., Zhang, Z., Zhu, Z., Lin, S., and Zhang, B. (2008).
1228 Visualization of monoaminergic neurons and neurotoxicity of MPTP in live transgenic zebrafish.
1229 *Dev. Biol.* 314, 84–92.
1230 Zhu, J.-N., and Wang, J.-J. (2008). The cerebellum in feeding control: possible function and
1231 mechanism. *Cell. Mol. Neurobiol.* 28, 469–478.
1232
1233
1234